Aalto University
School of Chemical
Technology

School of Chemical Technology
International Master's Programme in Bioproduct Technology

Meri Lundahl

END-FUNCTIONALIZATION OF CELLULOSE NANOCRYSTALS

Master's thesis for the degree of Master of Science in Technology submitted for inspection, Espoo, 14 May, 2014.

Supervisor **Professor Janne Laine**

Instructor **Dr. Lokanathan Arcot**

Aalto University
School of Chemical
Technology

Aalto University, P.O. BOX 11000,
00076 AALTO
www.aalto.fi

Abstract of master's thesis

Author Meri Lundahl

Title of thesis End-Functionalization of Cellulose Nanocrystals

Department Forest Products

Professorship Forest Products Chemistry **Code of professorship** Puu-19

Thesis supervisor Janne Laine

Thesis advisor(s) / Thesis examiner(s) Lokanathan Arcot

Date 14.05.2014 **Number of pages** 61+2 **Language** English

Abstract

Regioselective modification of nanocelluloses can have intriguing applications in self-assembled material synthesis. In this thesis, cellulose nanocrystals (CNC) were selectively functionalized at their reducing ends with thiol and maleimide groups. For thiol end-functionalization, a protocol was developed based on NHS/EDC-catalyzed coupling of $NaClO_2$-oxidized CNCs with NH_2-$(CH_2)_6$-SH in water. Maleimide end-functionalization was achieved by reacting end-thiolated CNCs (CNC-SH) with a homobifunctional maleimide crosslinker in ethanol.

Among the alternative protocols compared, end-thiolation was found to proceed most effectively in high ionic strength, with an EDC:NHS molar ratio of 10:1. Thus prepared CNC-SH adsorbed on gold as a fairly flexible layer in quartz-crystal microbalance with dissipation (QCM-D). Complying with a previous study, these results validate CNC-SH preparation via a faster reaction in simpler conditions than before. The results of maleimide end-functionalization suggested 50:1 as the optimal molar ratio between the maleimide crosslinker and thiols of CNC-SH. This modification lead to a slight adsorption of this sample on a surface covered with thiol groups in QCM-D. However, the adsorption remained low, probably due to limited yield of the functionalization.

In the future, control experiments are necessary to adequately validate the developed end-thiolation method. In addition, the maleimide end-functionalization needs to be more thoroughly optimized, particularly in ethanol media. With these improvements, both functionalization techniques could become feasible routes to prepare CNCs that attach to other molecules and surfaces in a controlled orientation.

Keywords cellulose nanocrystals, reducing end, functionalization

Preface

This thesis was completed in FuBio Cellulose project funded by the Finnish Bioeconomy Cluster (FIBIC).

I am enormously thankful for the supervision of Professor Janne Laine. Firstly, you have helped me to stay both focused on the essential work at hand and ambitious about the possible achievements in the field. Secondly, your attitude beautifully supports both high-quality research and a warm and free group atmosphere. As a result, you have consistently convinced me that I can achieve even more than I would otherwise believe.

My countless thanks belong to my thesis instructor, Dr. Lokanathan Arcot, for being tirelessly available and answering all my questions with enthusiasm. It has been totally inspiring to work with you and absorb some of the excitement with which you approach research. It is priceless to me how your support to my individual thinking and belief that I can find my own way have helped me develop into a better version of myself.

I had a great pleasure to receive practical help with my experiments from several wonderful people, such as Ritva Kivelä, Anu Anttila, Marja Kärkkäinen, Rita Hatakka, Timo Ylönen, Alexey Khakalo and Khan Ahsan Uddin. I am grateful for the time with you, your extreme helpfulness, as well as all your knowledge, skills and experience that I have had a chance to learn from.

In addition, I have received priceless support from my friends at the university and especially in AIESEC. You bring me joy and remind me of my commitment to keep growing as a person. I am also very grateful to my triathlon team. Our past couple of years have been a beautiful renewal of an old friendship in the form of breaking through old personal limits.

Finally, I am thankful for the encouragement, caring and love from my family. You keep reminding me about what most matters in life and inspiring me to live it fully and with integrity. Especially, my husband and best friend Lauri has been a constant source of support and joy. Thank you for sharing all these and future days with me and being an immensely good person.

Espoo, 14 May, 2014

Meri Lundahl

Table of Contents

Main abbreviations

NH_2-R-SH	6-amino-1-hexanethiol hydrochloride
AFM	Atomic force microscopy
BM-PEG	Bismaleimide-poly(ethylene glycol)
CNC	Cellulose nanocrystal
CNC-COO^-	Sodium chlorite oxidized cellulose nanocrystal
CNC-MAL	Cellulose nanocrystal end-functionalized with maleimide groups
CNC-SH	Cellulose nanocrystal end-functionalized with thiol groups
EDC	*N*-(3-Dimethylaminopropyl)-*N*′-ethylcarbodiimide hydrochloride
MQ	MilliQ water
NHS	*N*-hydroxysuccinimide
PNIPAAm	Poly(*N*-isopropyl acrylamide)
PTMP	Pentaerythritol tetrakis(3-mercaptopropionate)
QCM-D	Quartz crystal microbalance with dissipation

1. Introduction

Mimicking the hierarchical bottom-up fabrication method of natural materials is widely considered a promising approach to meet the current demand for sustainable and functional materials. Producing materials from the bottom up requires structural units expressing both the functionalities necessary for the application and the ability to interact with each other to form a precise architecture. In natural materials, the well-defined functionalities and architectures are enabled by a high degree of anisotropy (i.e., asymmetry in structure and/or properties) in the material components. This anisotropy applies to the components at all levels of the structural hierarchy: from the molecular level (components smaller than nanometer scale) through the colloidal level (components in nanometer scale) up to the macroscopic level (components in micrometer scale and larger) (Evans & Wennerström 1999).

At the bottom of the hierarchy, on the molecular level, small anisotropic molecules (e.g., amino acids, monosaccharides, nucleotides) are designed to asymmetrically react with corresponding molecular components. Thus, these small components are capable of forming anisotropic colloidal particles, including proteins, polysaccharides and nucleic acids. Up in the structural hierarchy, at the colloidal level, these particles can assemble into larger supramolecular architectures, guided by asymmetrically oriented interparticle interactions. Natural supramolecular architectures of colloidal building blocks can be bound together by covalent or non-covalent interactions. Non-covalent binding, such as electrostatic or van der Waals interactions, is preferable because of its facile reversibility and ability to transform at varying conditions. These dynamic connections provide for the natural architectures not only a precise organization but also a variable arrangement that can be programmed to serve life-sustaining processes (Mao, Xu & Wang 2010). Various supramolecular architectures assemble, in turn, into consecutively larger systems at the macroscopic level on the top of the structural hierarchy, eventually forming whole organisms.

A large and growing body of literature has investigated methods to engineer this kind of hierarchical self-assembly to synthetically fabricate as well-defined materials as the natural ones. Several molecular-level applications have already achieved a widespread use. For example, ordinary detergents consist of surfactant molecules that self-assemble

into colloidal micelles and onto macroscopic surfaces, building on the amphiphilicity (i.e., anisotropy between the hydrophilic and hydrophobic sections) in the molecule. On the next level, however, self-assembly of colloids poses a more difficult engineering challenge. The simplest solution uses the native tendencies of certain isotropic colloidal particles to assemble at interfaces or pack into liquid crystalline structures (Mao, Xu & Wang 2010). However, the complexity of these assemblies remains far from the level of natural supramolecular architectures. To mimic the natural fabrication process more closely, particles must combine their colloidal scale dimension with distinct anisotropy. The anisotropy can arise from a number of inconsistencies, including large aspect ratio (e.g., rod-like instead of spherical particle shape); spatially distributed reactivities; dipolarity (i.e., spatially distributed charges); or amphiphilicity. Amphiphilicity represents a particularly interesting source of anisotropy because amphiphilic colloids directly imitate the widely applied surfactant molecules on a larger scale.

The past decade has seen rapid progress in methods to engineer amphiphilicity in colloidal particles, as reviewed by Walther and Müller (Walther & Müller 2013). Their review presents three main possibilities to synthesize organic amphiphilic colloids. In general, the wettability on one side of a particle can be specifically modified by physically shading the other side. Alternatively, certain macromolecules (e.g., dendrons, block or graft copolymers) and supramolecular aggregates (e.g., micelles or polymeric precipitates) can be directly synthesized to contain distinct hydrophilic and hydrophobic domains. The third possibility involves isolating or biotechnically producing naturally anisotropic particles, such as proteins. The acquired particles are rendered amphiphilic if necessary and engineered further to fit the intended application. This route is considered especially promising, as it uses natural macromolecules as a raw material, thus enabling renewable and biocompatible applications. Among natural raw materials, particular attention is paid to cellulose because of its abundant availability. Cellulose is produced as a load-bearing component in many organisms, including plants, certain fungi, algae and bacteria, as well as the sea animal tunicate. In these organisms, cellulose acts as a reinforcing agent in composite materials formed with other molecules. For example, in wood, cellulose assembles with hemicelluloses and lignin into a composite structure with superior properties compared to each of its components. Due to the complexity of its native form, cellulose requires two rounds of processing to

become applicable for colloidal self-assembly. Firstly, cellulose needs to be extracted from its original composite form into nanoscale units. Secondly, these units need to be modified into a form that will correctly assemble with new particles, towards which cellulose often lacks the affinity that it natively displays towards hemicelluloses and lignin.

For the primary cellulose nanoparticle extraction, effective methods are already available and extensively reviewed (Klemm et al. 2011, Moon et al. 2011, Habibi, Lucia & Rojas 2010). The modification of the acquired nanocellulose can be realized by functionalizing cellulose into a form with affinity towards the other particles in the assembly. Unlike other hydrophilic substances, among which cellulose naturally tends to disperse, hydrophobic matrices pose a challenge to modify cellulose into a compatible form via hydrophobization. While numerous efforts have been directed at hydrophobizing the whole surface of cellulose nanofibrils or crystals (Moon et al. 2011), few studies have created localized amphiphilicity by hydrophobizing a limited region of the cellulose nanoparticle.

Yet, distinctly amphiphilic CNCs could enable the formation of various intriguing structures. For example, a hydrophobic surface could be covered with a layer of CNC rods oriented outwards. Using graphene as the hydrophobic surface could result in a similar composite to one developed earlier between graphene and cellulose nanofibrils (Laaksonen et al. 2011), except for the cellulose phase consisting of purely crystalline cellulose with controlled orientation in relation to the graphene sheets. Furthermore, in addition to static materials, amphiphilic CNCs could be employed in dynamic processes, such as forming micelles of colloidal particles for controlled drug delivery.

This thesis focuses on selective hydrophobization of the reducing ends of CNCs via conjugation with a hydrophobin-type protein. Hydrophobins contain a distinct hydrophobic domain, which causes these proteins to assemble at interfaces as amphiphiles (Linder 2009). Furthermore, a protein variant of hydrophobin II with a free thiol group has been shown to react with a dendron containing a free maleimide group while still retaining its affinity towards a hydrophobic surface (Kostiainen et al. 2006). Therefore, functionalization with maleimide was selected as the method to prepare CNCs for the protein conjugation.

While maleimide functionalization has been applied to conjugate various biomolecules with synthetic polymers (Hall, Van Den Berghe & Dove 2011, Li et al. 2010a) and fluorescent dyes (Cai et al. 2006), its application to cellulose has been poorly documented. The aim of this thesis is to functionalize the reducing end of a CNC with maleimide groups and verify the success of the functionalization as well as its intermediate reactions. The functionalization is performed via two steps as presented in Figure 1. The first step (Figure 1a) functionalizes the CNC reducing end with thiol groups, yielding an intermediate (CNC-SH) that is reactive with maleimide. The second step (Figure 1b) reacts the introduced thiol end groups with a homobifunctional maleimide crosslinker. The crosslinker includes two available maleimide groups: one to react with a thiol of CNC-SH, the other to remain available for protein conjugation. Thus, the end thiols are converted to end maleimides, resulting in a product (CNC-MAL) with reactivity towards thiol groups.

The first step is performed via two methods: reductive amination and NHS/EDC-catalyzed coupling. The protocol for CNC thiolation via reductive amination has been established elsewhere (Lokanathan et al. 2013). This thesis aims to develop a simpler alternative for CNC thiolation using NHS/EDC-catalysis to couple oxidized CNCs ($CNC\text{-}COO^-$) with a reagent including both an amine and a thiol group. In addition, this thesis develops a protocol for the second step; i.e., conversion of CNC-SH to CNC-MAL. The results are validated by applying three techniques: quartz crystal microbalance with dissipation (QCM-D), atomic force microscopy (AFM) and Ellman's assay. QCM-D examines on one hand the tendency of CNC-SH to bind to gold, on the other hand the reactivity of CNC-MAL with a thiol-covered surface. AFM provides visual information about the adsorbed samples on the QCM-D crystal surface. Ellman's assay can approximately quantify the amount of thiol or maleimide groups in CNC by utilizing the reactivity of thiol groups with a colorimetric reagent.

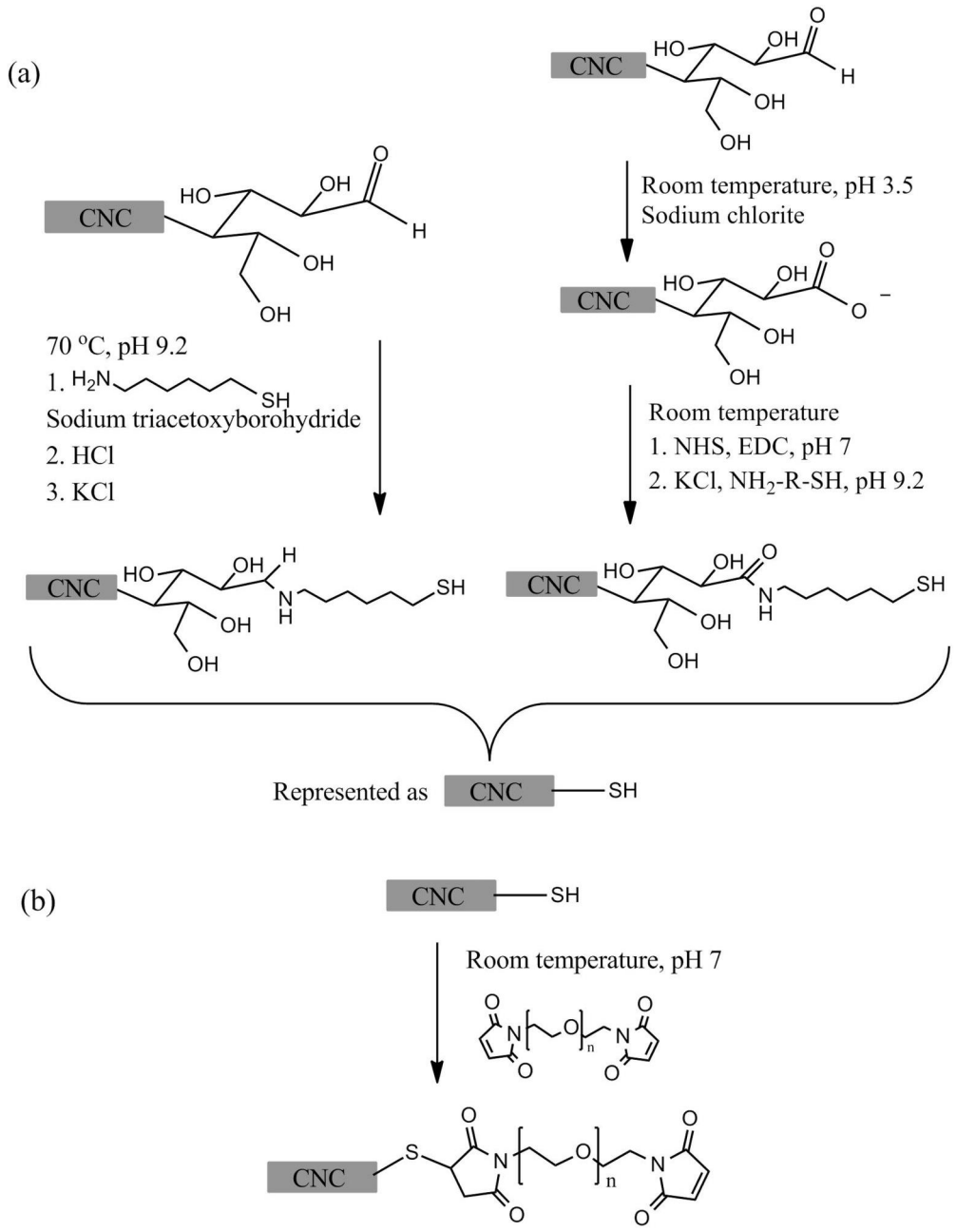

Figure 1: Schematic representation of the subsequent reactions: (a) CNC reducing end thiolation performed via (left) reductive amination or (right) NHS/EDC-catalyzed coupling, and (b) conversion of end thiol to maleimide.

2. Literature Review

This chapter aims to identify the most feasible opportunities to develop self-assembling colloidal structures utilizing cellulose as a raw material. Section 2.1 provides examples on attempts to introduce amphiphilic behavior into natively isotropic macromolecules. Section 2.2 discusses the chemical characteristics of cellulose and how they have been exploited to induce self-assembly. Surface active properties of CNCs and opportunities to chemically enhance them are reviewed in Section 2.3.

2.1 Colloidal Self-Assembly

A tendency for self-assembly is found in many colloidal particles. As long as the particles have a colloidal size and only moderate hydrophilicity or hydrophobicity, they energetically prefer to assemble at interfaces where they lower the surface tension and can even stabilize foams or emulsions (Mao, Xu & Wang 2010). Furthermore, when dispersed colloidal particles are monodisperse in terms of size, shape and chemical properties, they pack into a liquid crystalline structure upon slow sedimentation or controlled solvent removal (Mao, Xu & Wang 2010). On the other hand, provided that the colloids are isotropically hydrophilic or hydrophobic, they are unable to aggregate into more complex and reversible supramolecular architectures, such as micelles or vesicles (Mao, Xu & Wang 2010). This behavior is enabled by amphiphilicity.

Amphiphilicity can be artificially created by selectively modifying particles from a certain direction only; by selecting molecular components that form amphiphilic particles under correct conditions or events; or by using natively amphiphilic particles (e.g., amphiphilic biomacromolecules) as a basis for further engineering. The self-assembly of synthetic, amphiphilic particles can be influenced by altering the sizes, strengths and separation of the hydrophilic and hydrophobic domains in the individual particles (Walther & Müller 2013). Synthetic self-assembly building blocks can even be designed to dynamically respond to a variety of external cues, including not only temperature, pH, humidity and light, but also external electric or magnetic fields (Walther & Müller 2013). This section introduces a selection from the wide range of examples on artificial colloidal self-assembly.

Hong and co-workers applied the surface activity of colloidal particles to immobilize silica spheres at the interface between paraffin and water (Figure 2a), exposing to chemical modification only the hemisphere facing the water phase (Hong, Jiang & Granick 2006). An oil-in-water emulsion has a multiple times larger interfacial surface area than the planar interfaces utilized earlier for colloid shading. Therefore, this method enabled scaling up the amount of particles that can simultaneously be direction-specifically modified using the physical shielding approach. After covering the exposed hemisphere with a fluorescent cationic coating and the shaded hemisphere with hydrophobic coating, the silica spheres, unlike unmodified silica, adsorbed on a hydrophobic surface. The adsorbed spheres also expressed fluorescence, suggesting that both applied coatings were present on the particles (Hong, Jiang & Granick 2006). The relative sizes of the hydrophilic and hydrophobic regions (corresponding to hydrophilic-lipophilic balance of molecular-sized surfactants) could be adjusted by using a surfactant to allow the silica spheres sink deeper into the oil phase of the emulsion (Jiang & Granick 2008).

Similar technique has been applied to coating one hemisphere of a silica sphere with polyacrylamide and the other with polystyrene, yielding colloids that selectively adsorbed hydrophilic metallic nanoparticles on the polyacrylamide-coated hemisphere (Liu et al. 2008). A smaller and even more efficiently produced version of a similar colloid was prepared in a styrene-in-water emulsion, using poly(methacrylate acid) as the hydrophilic coating (Zhang, Jin & Zhao 2009). These particles were observed not only to adsorb hydrophilic particles on the poly(methacrylate acid)-coated hemisphere (Figure 2b) but also to assemble into aggregates that shield the insoluble hemisphere from a selective solvent.

Even though emulsions offer a large interfacial area for particle shading, only a limited amount of particles can be processed at a time in a static fluid. Scalable production of amphiphilic colloids can more feasibly be achieved by microfluidics. A microfluidic device processes a continuous stream of raw material while still producing particles with highly controlled shapes and functionalities (Dendukuri, Hatton & Doyle 2007). Dendukuri and co-workers directed through a microfluidic device parallel flows of tri(methylolpropane) triacrylate (TMPTA) and an aqueous solution of poly(ethylene

glycol) diacrylate (PEG-DA) (Dendukuri, Hatton & Doyle 2007). Both PEG-DA and TMPTA polymerize upon UV exposure. These neighboring flows were passed over a beam of UV light covered by a wedge-shaped mask. Thus, wedge-shaped polymeric particles were formed with one hydrophobic side consisting of polymerized TMPTA and another hydrophilic side polymerized of PEG-DA. The amphiphilic polymer wedges were shown to act as giant surfactants in solutions and emulsions (Figure 2c). Nie et al. applied similar technique without masking the UV light (Nie et al. 2006). Instead, these authors used a microfluidic device that causes such a high sheer on the parallel monomer streams that these break into droplets with hydrophilic and hydrophobic compartments. This droplet morphology was sealed under UV light when the monomers polymerized. The resulting amphiphilic polymer spheres assembled in a selective solvent into micelle-like structures (Figure 2d) that could be altered by adjusting the balance between the hydrophilic and hydrophobic volumes in the monomer droplets.

Besides UV light, the amphiphilic particle formation may be triggered by other signals, such as solvent evaporation (Walther & Müller 2013). Even without this kind of external signals, several synthetic procedures can be executed, provided that the correct conditions and reagents are available. The most traditional example on this involves block copolymer synthesis from hydrophilic and hydrophobic monomers (Zhao et al. 2013). However, block copolymers verge between molecules and colloids, thus often lacking the properties of a colloidal particle (Walther & Müller 2013). Therefore, block copolymers have increasingly been replaced by more novel alternatives, such as complexes of homopolymers, random and graft copolymers, dendrons as well as hyperbranched polymers (Zhao et al. 2013).

Wei and co-workers polymerized poly(*N*-isopropyl acrylamide) (PNIPAAm) between a carboxylic group and a short hydrocarbon chain (Wei et al. 2011). The acquired amphiphilic polymer formed micelles in water with a hydrocarbon core at temperatures below 34 ^{o}C, when PNIPAAm exists in coil conformation. Above 34 ^{o}C, when PNIPAAm collapses, the micelles fuse into larger vesicles to minimize the surface energy between PNIPAAm and water. This transformation upon temperature cue was essentially reversible and quick especially to the reverse direction. This was enabled by

adequately short hydrophobic tail. However, too limited hydrophobicity would prevent the vesicle formation and lead to precipitation.

Li et al. demonstrated micellization in selective solvent (Figure 2e) of a block-graft copolymer with polystyrene side chains on one block and poly(*tert*-butyl acrylate) side chains on the other block (Li et al. 2010b). Ariura and co-workers observed corresponding behavior depending on solvent and support (Figure 2f) in a similar polymer with methyl vinyl ether replacing *tert*-butyl acrylate as the hydrophilic monomer (Ariura et al. 2009). Even a similar polymer with randomly distributed polystyrene and poly(methyl vinyl ether) side chains could self-assemble into lamellar structures upon solvent evaporation for thin film preparation (Lanson et al. 2009).

Chen et al. applied the difference in reactivity between the focal point and branch terminals of poly(amido amine) dendron with a propargyl focal point and four primary amine terminal groups (Chen et al. 2013). These authors selectively attached a polypeptide of lysine at the focal point and a polypeptide of glutamate at each branch. The hydrophilicity of the attached polypeptide chains was pH-responsive, increasing when the chain was charged. Therefore, this macromolecule self-assembled into various formations depending on pH, shielding the uncharged regions with charged ones, also influenced by the steric effect of the branches.

Another example based on dendrons was published by Zou et al., concerning functionalization of the focal point of a Frechét-type benzyl ether dendron with an azobenzene group (Zou et al. 2009). The functionalized dendron was mixed with β-cyclodextrin end-functionalized PNIPAAm and transferred to water where the azobenzene and β-cyclodextrin complexed. Thus, a complex of PNIPAAm and a hydrophobic dendron was formed that self-assembled at room temperature into vesicles with PNIPAAm at both outer and inner layers shielding the dendrons in between. Upon exposure to UV light, azobenzene changed conformation thus breaking the complex and changing the vesicular structure into more irregular aggregates. Approximately original vesicular assembly was recoverable via exposure to visible light. The vesicles could also be reversibly aggregated by increasing the temperature, thus decreasing the hydrophilicity of PNIPAAm.

In addition to complexation with azobenzenes, cyclodextrins can be covalently functionalized into amphiphilic macromolecules. In this case, cyclodextrin functions like a dendron, providing a platform for several substituents to diverge from. Unlike a dendron with a single focal point, though, cyclodextrin includes several hydroxyl groups available for selective modification on each side of a ring of glucose units. This underlying structure tends to effectively hold the substituents separated without the need for extreme chemical incompatibility between them (Walther & Müller 2013). Ge and co-workers capitalized on this advantage of cyclodextrins to engineer self-assembled structures with two hydrophilic polymers (Ge et al. 2009). These authors introduced 14 PNIPAAm chains on one side and 7 poly[2-(diethylamino)ethyl methacrylate] (PDEA) chains on the other side of β-cyclodextrin. In aqueous solution at a temperature above 34 ^{o}C and a pH below 6, when PNIPAAm is insoluble and PDEA soluble, vesicular arrangement was observed with PDEA coronas around a PNIPAAm bilayer. The vesicles were inverted when temperature was decreased and pH increased (Figure 2g). Mazzaglia et al. prepared vesicles based on more clearly amphiphilic β-cyclodextrin with separated thioalkyl and oligo(ethylene oxide) chains (Mazzaglia et al. 2013). This amphiphilic cyclodextrin was also complexed with a hydrophobic drug molecule to study the applicability of a vesicle as a drug carrier.

Like dendrons and cyclodextrins, numerous biomacromolecules possess native anisotropy that can be utilized for selective functionalization. Certain biomolecules are even naturally amphiphilic and thus require only minor processing to be used in applications targeting self-assembly mediated by hydrophobic interactions. Especially a class of fungal proteins called hydrophobins has aroused extensive interest because of their well-defined amphiphilicity and self-assembly patterns (Walther & Müller 2013). Varjonen and co-workers genetically modified a class II hydrophobin into a fusion protein featuring two cellulose binding domains similar to those present in fungal cellulose-degrading enzymes (Varjonen et al. 2011). The acquired fusion protein bound to hydrophilic cellulose at the cellulose binding domains and to hydrophobic surfaces at the hydrophobic domain of hydrophobin. This property enabled cellulose nanofribril attachment to oil droplets in water for emulsion stabilization (Varjonen et al. 2011) or to graphene sheets for nanocomposite material formation (Laaksonen et al. 2011).

Images from selected self-assembly studies reviewed in this section are provided in Figure 2. Among the extensive literature about this topic, the examples based on protein-cellulose complexes are particularly promising, since they utilize renewable and biocompatible raw materials while being impressively versatile. A wide range of combinations could be created with proteins delivering selected functionalities and cellulose adding mechanical strength. Besides non-covalent complexation, a variety of covalent modifications can be applied to cellulose in order to develop it into a suitable component for self-assembly. These opportunities are reviewed in the next section.

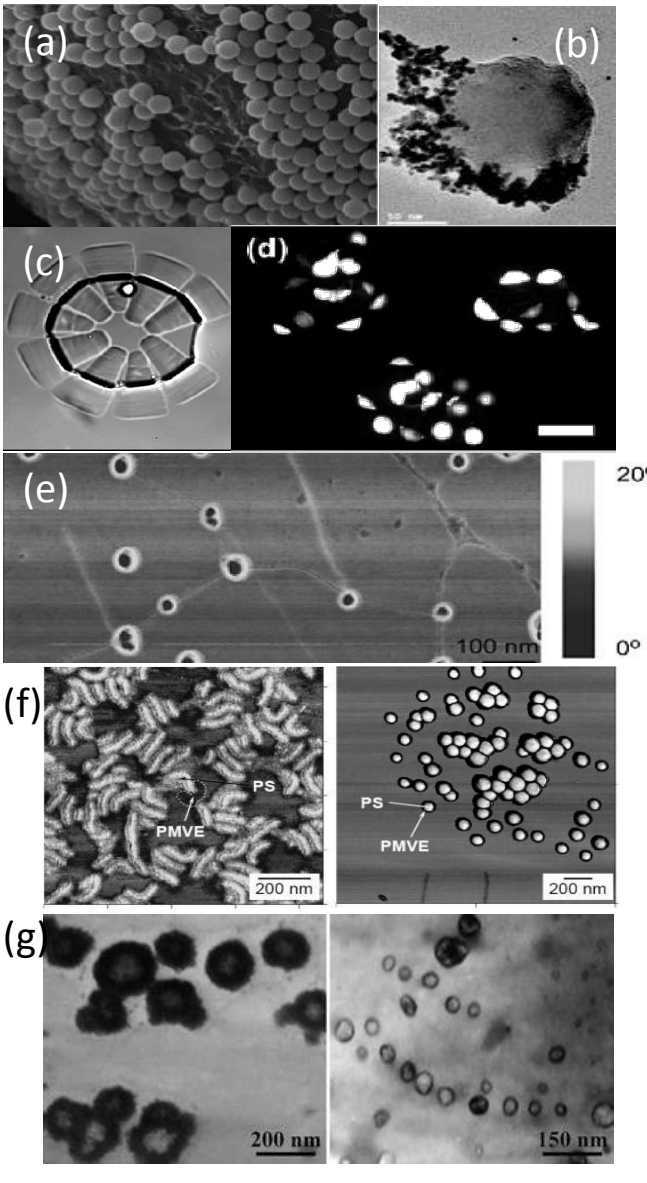

Figure 2: Selected images of examples on synthetic colloidal self-assembly:

(a) scanning electron micrograph of silica spheres at paraffin-water interface in preparation for regio-specific modification in emulsion (Hong, Jiang & Granick 2006)

(b) scanning electron micrograph of gold nanoparticles prepared in clusters complexed with the hydrophilic region of an amphiphilic silica sphere (Zhang, Jin & Zhao 2009)

(c) assembly of amphiphilic polymer wedges around an oil droplet in water (Dendukuri, Hatton & Doyle 2007)

(d) fluorescent micrograph of aggregates of amphiphilic polymer spheres (Nie et al. 2006):

(e) AFM image of micelles formed by an amphiphilic block-graft copolymer (Li et al. 2010b)

(f) AFM phase images of the adjustable arrangement of an amphiphilic block-graft copolymer from CH2Cl2 on highly oriented pyrolytic graphite (left) and from methanol on mica (right) (Ariura et al. 2009):

(g) transmission electron micrographs of the inversible vesicles of cyclodextrins substituted with PDEA (darker) and PNIPAAm (lighter) at pH 4 and 45 °C (left) and pH 10 and 25 °C (right) (Ge et al. 2009)

2.2 Chemistry and Self-Assembly of Cellulose

Cellulose is a promising raw material for building units for colloidal self-assembly not only because of its sustainability but also its chemical versatility. As illustrated in Figure 3, cellulose is a chain of β-D-glucopyranose monomers, each consecutive monomer rotated 180° with respect to the neighboring ones. Together, two β-D-glucopyranose rings form a cellobiose, which is the repeating unit of cellulose. Regardless, the degree of polymerization (DP) of cellulose is defined as the total amount of individual β-D-glucopyranose monomers. Each of these monomers is slightly amphiphilic (Yamane et al. 2006). Hydrophilicity is situated at the equatorial direction of the β-D-glucopyranose ring, arising from the hydroxyl groups that can hydrogen bond to neighboring rings, including those in neighboring chains. Hydrophobicity originates from the carbon-hydrogen bonds along the axial direction. Together, the hydrogen bonds and hydrophobic interactions cause cellulose to assemble into fibrils with tightly packed crystalline regions. The amphiphilicity between the equatorial and axial directions along cellulose chain has also been shown to enable applying cellulose as a dispersing agent (Rein, Khalfin & Cohen 2012, Kalashnikova et al. 2011). However, more complicated self-assembly applications require modifying the cellulose material to exaggerate its amphiphilic qualities. This can occur via non-covalent binding of a suitable adsorbate or via covalent attachment of new functionalities (Moon et al. 2011). This review focuses on the covalent modification methods.

A cellulose chain (Figure 3) provides two types of reactive sites for covalent modification: hydroxyl groups and a hemiacetal group. Hydroxyl groups are attached to C2, C3 and C6 of each glucose monomer as well as C4 of the terminal glucose unit in the nonreducing end. The hydroxyl groups along the chain can participate in a number of reactions, including oxidation (Azzam et al. 2010), esterification (Zoppe et al. 2010, Habibi et al. 2008), etherification with alkylating agents (Hermanson 1996) and reaction with isocyanates (Taipina et al. 2013, Shang et al. 2013, Yu & Qin 2014). The basic reactions can be used as a basis for a variety of cellulose functionalization methods. In other words, pristine cellulose, partly functionalized cellulose or cellulose derivatives can be further functionalized or even grafted with another macromolecule. As an

alternative to grafting a full molecule onto the cellulose chain, the chain can be functionalized with a polymerization initiator enabling polymer grafting from cellulose outwards, monomer by monomer. Depending on the intended functionalization or grafting protocol, a starting material is selected with appropriate reactivity (Hebeish & Guthrie 1981).

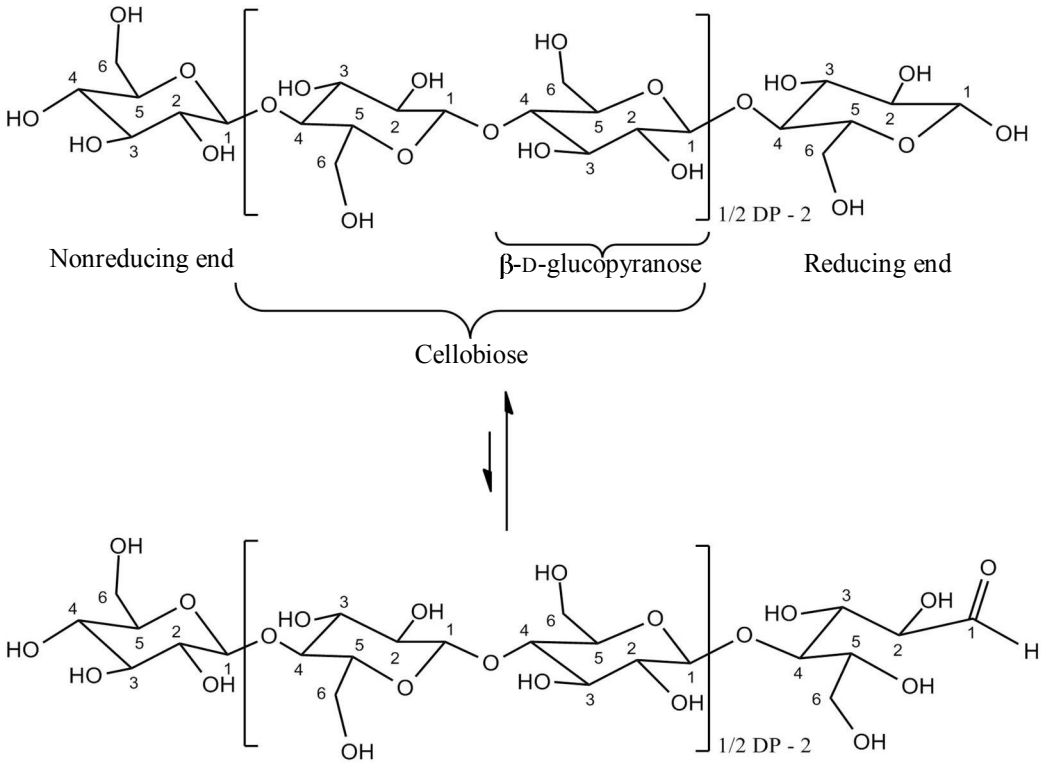

Figure 3: Chemical structure of the alternative forms of cellulose.

Unlike hydroxyl groups, a hemiacetal only exists in the reducing end of a cellulose molecule. The terminal monomers in this end exist in equilibrium between their ring form and open form (Figure 3). While open, the terminal monomer reacts as an aldehyde with amine or hydrazine functionalities (Hermanson 1996). These reactions proceed slowly and can take more than a week to produce a considerable yield, due to the rare availability of the aldehydes (Hermanson 1996). Nevertheless, this route enables a highly regioselective functionalization method for cellulose. An alternative route to end-specific functionalization utilizes cellulose derivatives with all their hydroxyl groups substituted, including those at C1 of reducing and C4 at nonreducing end. For example, in cellulose triacetate, either terminal acetate group can be

regioselectively reacted because of their different chemical environments compared to other acetates in the molecule (Kamitakahara & Nakatsubo 2005, Arndt et al. 2003).

An extensive amount of literature has described various chemical modifications of the cellulose surface hydroxyl groups (Hebeish & Guthrie 1981). In addition, a number of studies have been published on regioselective cellulose end-functionalization. For example, Glasser and Becker (Glasser & Becker 1999) demonstrated that when depolymerizing cellulose propionate with HBr in an aprotic solvent, the propionate groups at C1 in the reducing end can be substituted by bromine. This promotes branching of the cellulose propionate chain due to the reactivity between the bromine and hydroxyl groups (Glasser & Becker 1999).

Kasuya and co-workers (Kasuya et al. 2002) adopted reductive amination to link silica gel to low-molecular-weight cellulose prepared via a mild, 6-week-long phosphoric acid hydrolysis. A chiral stationary phase was obtained for high-performance liquid chromatography with improved solvent compatibility and competitive chiral separation capacity. More recently, Velleste et al. (Velleste, Teugjas & Väljamäe 2010) labelled various types of cellulose with 2-aminobenzoic acid via reductive amination. The labelled celluloses were used to determine the directional preferences of cellulose-degrading enzymes. For this purpose, regenerated cellulose with low DP was discovered to serve best because of its high reducing end content (Velleste, Teugjas & Väljamäe 2010).

Kamitakahara and Nakatsubo (Kamitakahara & Nakatsubo 2005) replaced acetate groups in the reducing ends of cellulose triacetate (CTA) with azide groups. The introduced azides were reduced into amine form and reacted with a hydrophobic carboxylic acid. Thus, a hydrophobic section was attached to the CTA via an amide bond. The added carboxylic acid contained an azide group at the other end of its hydrophobic chain, enabling the repetition of the same reaction in cycles. Thus, the amount of hydrophobicity could be controlled in the resulting amphiphile. Finally, the remaining acetate groups were removed to recover the hydrophilicity of the cellulose domain. Similar technique has been elaborated on and applied to several aspirations, such as grafting cellulose onto a poly(methyl methacrylate) backbone (Enomoto-Rogers et al. 2012); forming radially oriented cellulose shells around gold nanoparticles

(Enomoto-Rogers et al. 2011a); micelle-like self-assembly of cellulose end-functionalised with a hydrophobic alkyl chain and a pyrene label (Enomoto-Rogers et al. 2011b); as well as attaching cellulose to methylcellulose that has been regioselectively functionalized to contain an azide-reactive nonreducing end (Nakagawa, Kamitakahara & Takano 2012). The cellulose-methylcellulose diblock copolymer was even observed to form hydrogels, the molecular architecture and strength of which varied with temperature and the size of the hydrophilic cellulose block (Nakagawa et al. 2012).

However, the applications presented above are limited to cellulose derivatives as a starting material. The structural properties of cellulose and its derivatives are radically different. For example, if the crystalline properties of native cellulose are required for an application, the cellulosic material itself needs to suffice as a starting material without derivatization. In the case of macroscopic cellulose fibers or cellulose nanofibrils, the starting material needs to retain its partial crystallinity throughout the processing. In the case of CNCs, the partial crystallinity has already been altered by removing amorphous sections of native cellulose, leaving only crystalline sections in the material. The following section focuses on methods that preserve this crystallinity while developing CNCs towards artificial self-assembly.

2.3 Self-Assembly of Cellulose Nanocrystals

The monomers of cellulose (Figure 3) are connected with such strong β-1,4 glycosidic linkages that they can only be separated via specialized enzymes or harsh acid hydrolysis. Furthermore, the hydroxyl groups around the β-D-glucopyranose rings tend to form both inter-chain and intra-chain hydrogen bonds (Figure 4a). This hydrogen bonding, accompanied by van der Waals forces between the hydrophobic ring axes, induces such tight crystalline packing that even acid treatment, unless prolonged, scarcely affects the crystalline regions. When this difference between acid treatment kinetics at crystalline and amorphous cellulose regions is used to selectively degrade amorphous cellulose, CNCs are obtained (Figure 4b). In this process, the DP of cellulose decreases dramatically. The native DP of 20 000 has already decreased during initial processing and CNC production reduces it further down to only several hundreds

or thousands, for a less or more crystalline raw material, respectively (Habibi, Lucia & Rojas 2010). These DP values correspond to CNC lengths of few hundred nanometers or few micrometers (Klemm et al. 2011). Concerning length, however, especially long CNCs are often polydisperse (Habibi, Lucia & Rojas 2010). Nevertheless, the crystals maintain a relatively high aspect ratio with diameters limited to 5-70 nm (Klemm et al. 2011).

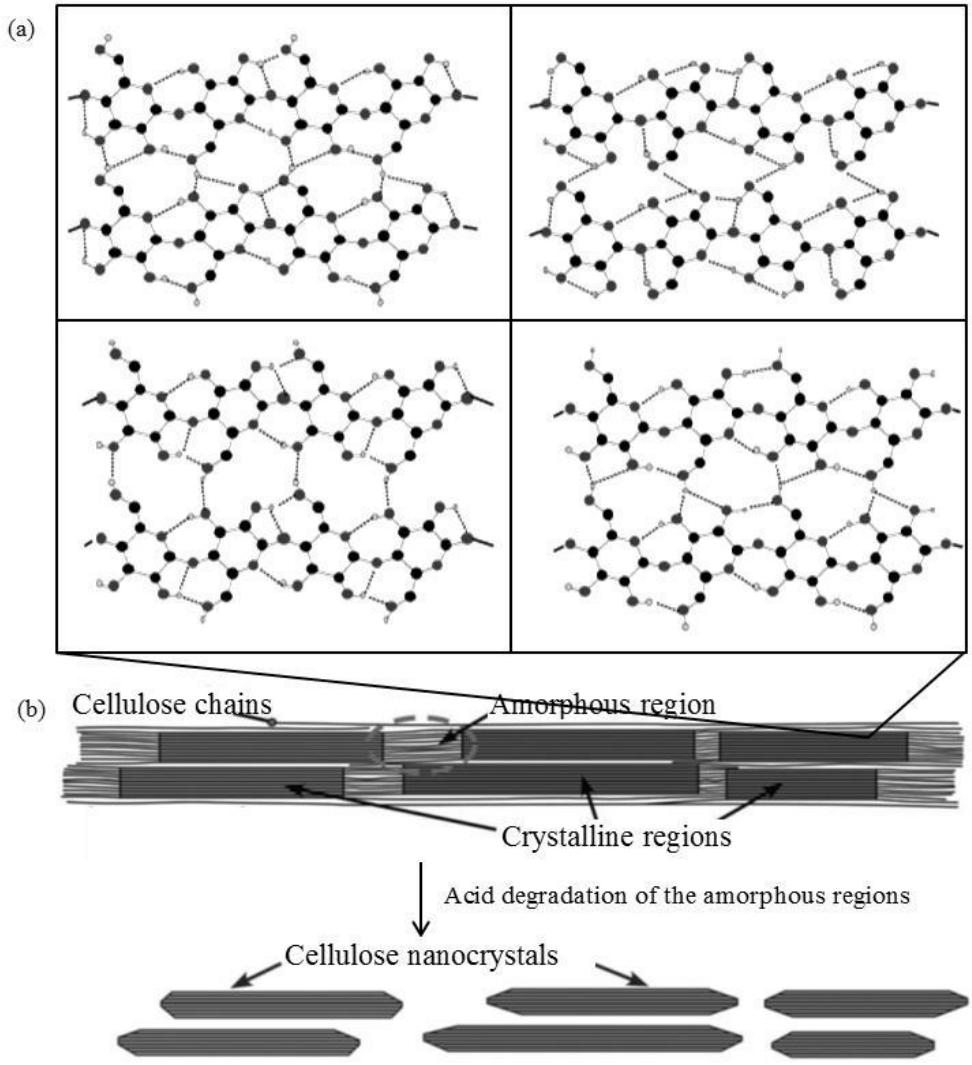

Figure 4: (a) Alternative hydrogen bonding patterns between adjacent cellulose chains in crystalline regions. An essential difference between the top (cellulose Iα) and bottom (cellulose Iβ) arrangements is caused by the difference in the stacking of the sheets of parallel cellulose chains upon each other. Adopted from (Sturcová et al. 2004). (b) Schematic arrangement of crystalline and amorphous domains in native cellulose and formation of CNCs, adopted from (Moon et al. 2011).

Besides the degree of crystallinity in the raw material determining the dimensions, CNC properties are influenced by their detailed preparation method. For example, longer acid treatment time produces shorter CNCs and higher degree of substitution on CNC surface. The substitute groups introduced on the surface are determined by the acid in use. For example, selecting hydrochloric acid leads to hydroxylated, acetic acid to acetylated, or sulfuric acid to sulfated crystal surfaces (Moon et al. 2011). Sulfuric acid is most commonly employed, since negatively charged sulfated surfaces repel each other strongly, thus effectively stabilizing a crystal suspension in water.

Regardless of the repulsion in CNC suspensions, these have a native ability to self-assemble into chiral nematic liquid crystalline structures (Klemm et al. 2011). This CNC property has been recently exploited by Kelly et al. to fabricate stained glass with varying optical properties (Kelly et al. 2012). Utilizing the effect of increasing ionic strength on tightening the chiral nematic structure of a CNC dispersion, these authors controlled the mesoporosity of CNC/silica composite films. The pores in these films were decorated with metal nanoparticles, which thus achieved varying interparticle separations (i.e., varying color). Another example of using the chiral nematic order of CNCs as a template for creating colors was published by Shopsowitz and co-workers (Shopsowitz, Hamad & MacLachlan 2012). In this study, composites of CNCs and organosilica were prepared containing the components in varying ratios. Altering the CNC-organosilica ratio also altered the separation between CNCs when forming a liquid crystal. When the CNCs were removed via strong acid treatment, correspondingly separated pores were left in the remaining organosilica framework. Differences in pore separation constituted differences in color.

Both the above examples rely on only one type of CNC arrangement. Alternative self-assembly patterns, such as dispersion in a hydrophobic polymer resin (Moon et al. 2011), may be induced by modifying the chemical properties of CNCs. However, applying chemical modifications to the CNC surface poses a risk of altering the crystal morphology (Habibi, Lucia & Rojas 2010), retention of which is often essential for guaranteeing the mechanical properties of the intended applications. Nevertheless, several CNC surface modifications have been performed essentially without damaging

the crystal structure while still achieving a new self-assembly pattern. Next, this section introduces a selection of these modifications.

Taipina and co-workers increased the compatibility of CNCs with a hydrophobic matrix via silylation, reacting the isocyanate groups of isocyanatepropyltriethoxysilane reagent with the crystal surface hydroxyls (Taipina et al. 2013). The ethyloxysilane groups of the reagent formed a polysilesquioxane network around the CNCs, shielding the hydrophilicity, which would otherwise cause aggregation in hydrophobic media. Another related CNC hydrophobization route was reported by Shang and co-workers (Shang et al. 2013), who grafted castor oil onto CNCs by connecting the hydroxyl groups on the CNC surface with the hydroxyl groups in castor oil molecules. The hydroxyl groups were attached via toluene diisocyanate. This molecule contains two isocyanate groups, which are reactive with hydroxyl. Firstly, one of these isocyanate groups was reacted with a castor oil molecule that had two of its three hydroxyl groups protected and one available for isocyanate. Secondly, the resulting isocyanate-activated castor oil was reacted with sulphuric acid hydrolyzed CNCs.

Toluene diisocyanate was also recently utilized by Yu and Qin (Yu & Qin 2014) to couple hydroxyl-activated poly(3-hydroxybutyrate-co-3-hydroxyvalerate) with CNC surface hydroxyls. They acquired a hydrophobic graft copolymer with tunable hydrophobicity: increasing grafting density and DP of the grafted polymers also increased the hydrophobicity. Furthermore, this grafting improved the thermal stability of CNCs, essentially upto a level that enables melt processing the copolymer like a plastic. In a related study, Habibi et al. developed plasticized CNCs by grafting poly(ε-caprolactone) (PCL) from the surface hydroxyls (Habibi et al. 2008). Through the PCL grafting, CNCs became a well dispersible reinforcing filler for a PCL matrix. Nanocomposites of PCL and PCL-grafted CNCs could be prepared by solvent casting (Habibi et al. 2008) or, to avoid using harmful solvents, by melt blending followed by injection molding (Goffina et al. 2011).

Numerous other examples on CNC hydrophobization exist but a significant proportion of them are beyond the scope of this literature review. Besides simply increasing compatibility with hydrophobic media, CNC modification can aim for stimuli-responsive self-assembly behavior. For example, Zoppe et al. demonstrated

thermoresponsive aggregation of CNCs grafted with PNIPAAm (Zoppe et al. 2011). This study highlighted that grafting a hydrophilic polymer on CNCs changes the primary mechanism for dispersion stabilization from electrostatic to steric repulsion. The (partial) collapse of PNIPAAm coils caused by increasing temperature and/or ionic strength weakens the steric repulsion and can break the dispersion (Zoppe et al. 2011). Corresponding aggregation can also be achieved by grafting other thermosensitive polymers, including copolymers of ethylene and propylene oxides (Azzam et al. 2010).

As explained in Section 2.2, the reducing end of a cellulose chain has unique chemical properties compared to the hydroxyl groups along the chain. This distinction has been applied to selectively modify the reducing ends of CNCs. Sipahi-Saglam et al. exploited the reactivity between aldehyde and hydrazine groups to attach crosslinkers or polymerization initiators to a CNC reducing end via hydrazone linkages (Sipahi-Saglam, Gelbrich & Gruber 2003). The selected crosslinker contained an available carboxylic group, which enabled the activated CNC to react with a macromolecule including a free amino group. The polymerization initiator, on the other hand, induced the grafting of poly(acryl amide) from the activated sites. Thus, via grafting-from polymerization of poly(acryl amide) or crosslinking with varying macromolecules, a selection of end-functionalized CNCs was acquired. Even hydrophobically associating CNC was produced by selecting a hydrophobic polymer as the end functionality (Sipahi-Saglam, Gelbrich & Gruber 2003).

The same technique was recently applied by Karaaslan and co-workers to conjugate CNC with beta-casein (Karaaslan, Gao & Kadla 2013). β-casein is an amphiphilic protein that arranges into micelles in aqueous environments. This implies that conjugates of this protein and CNC could also form micelles and even orient themselves at interfaces. However, in this study, β-casein attached to CNCs as ready-assembled micelles instead of individual proteins. Only few of these micelles had CNCs attached to several included proteins (Karaaslan, Gao & Kadla 2013). A conjugated closed micelle introduces no active hydrophobic functionality in a CNC due to the concealment of the hydrophobic areas inside the micelle. Thus, full utilization of the properties of a CNC-β-casein conjugate would require breaking of the original micellar structure and removal of the unconjugated proteins. Nevertheless, the presented concept of CNC

conjugation with β-casein could potentially be beneficial for several applications (e.g., bottom-up material fabrication, vesicles for targeted drug delivery) (Karaaslan, Gao & Kadla 2013).

In addition to hydrazines, aldehydes react with amine groups to form imines (Hermanson 1996). Already over decades, this reaction has been employed to detect carbonyl groups in polysaccharide samples by staining them with thiosemicarbazides (Ahn, Rhee & Stadtman 1987). This technique has also been applied to CNCs made of bacterial cellulose (Koyama et al. 1997). In this study, the CNCs were treated with thiosemicarbazide-silver proteinate, which includes an amine group to bond to an available CNC aldehyde and a silver tag that can be observed by electron microscopy. These tags were only visible at one end of each crystal, since in a crystal of bacterial cellulose, like in other natural celluloses, all cellulose chains are found in parallel arrangement. Thus, the tagging could even provide information about the orientation of the cellulose during its synthesis (Koyama et al. 1997).

Imines can be further stabilized by reducing them into amines via reductive amination (Hermanson 1996). This reaction was recently applied by Lokanathan et al. to end-functionalize CNC with thiol groups (Lokanathan et al. 2013). However, due to the poor availability of terminal glucose rings in their open form, this reaction requires an extended incubation time. Moreover, this study only achieved the end-functionalization at an elevated temperature. Nevertheless, the acquired CNC-SH was able to attach to noble metal surfaces and nanoparticles because of the chemical affinity between thiols and noble metals. Furthermore, the thiol groups make CNC-SH highly chemically versatile, since thiols react with a variety of functional groups, including haloacetyls, alkyl halides, maleimides, aziridines and disulfides (Hermanson 1996). Therefore, thiol end-functionalization can serve as a method to prepare a CNC for further functionalization or conjugation with a thiol-reactive molecule of choice.

Examples on alternative thiol-reactive molecules include not only functionalized macromolecules, such as proteins or even other CNCs, but also crosslinkers that introduce new functionalities. Li and co-workers crosslinked thiol end-functionalized PNIPAAm (PNIPAAm-SH) with bovine serum albumin and ovalbumin using 1,8-bis-maleimidodiethyleneglycol (BM-DEG) (Li et al. 2010a). BM-DEG features two

maleimide groups, one of which was first reacted with PNIPAAm-SH, achieving 80% conversion of the PNIPAAm-SH molecules to maleimide-terminated ones. The resulting maleimide end-functionalized PNIPAAm chains were coupled with free cysteine residues in the proteins, mostly retaining the protein activity. Furthermore, the acquired polymer-protein conjugates demonstrated thermoresponsive aggregation at temperatures favoring the collapse of PNIPAAm.

Yoshitake et al. conjugated glucose oxidase with different rabbit antibodies using a crosslinker with *N*-hydroxysuccinimide ester and maleimide groups (Yoshitake et al. 1979). Glucose oxidase was reacted first with the *N*-hydroxysuccinimide ester section in the crosslinker, after which the maleimide section was coupled with thiol groups made available in the antibodies by reduction. The enzymatic activity of the glucose oxidase decreased little and the antigen binding ability of the antibodies was essentially preserved upon conjugation.

The protein to be conjugated can also be selected to enable colloidal self-assembly of the resulting conjugate. Kostiainen and co-workers prepared an amphiphilic dendron-protein conjugate using a polyamine dendron with a maleimide group at the focal point and a protein variant of hydrophobin II including a free thiol group (Kostiainen et al. 2006). This conjugate was capable of binding to DNA at the dendron branches and to hydrophobic surfaces at the hydrophobic domain of the hydrophobin. These results imply that hydrophobins could likewise be conjugated with other molecules in order to add amphiphilicity to the functionality of the original molecule. In the case of CNC, an amphiphilic colloid with highly crystalline, reinforcing properties would be acquired. In addition, the surface hydroxyls of the hydrophobin-conjugated CNCs could be further functionalized to suit the intended application.

Hieta, Kuga and Usuda reported another approach to increase the chemical versatility of CNCs (Hieta, Kuga & Usuda 1984). This approach capitalized on the ability of the aldehydes present in the CNC reducing ends to be oxidized into carboxylates. After oxidation, the acquired end carboxylates could form salts with introduced silver ions, thus establishing nuclei for the formation of silver tags (Hieta, Kuga & Usuda 1984). Besides salt formation with anions, carboxylates can undergo other reactions, including NHS/EDC-catalyzed coupling as a widely applied example (Hermanson 1996). Among

various other targets, NHS/EDC activation has been used to modify carboxylates introduced on a cellulose nanofibril surface (Orelma et al. 2012). In this study, the NHS/EDC activation enabled the conjugation of proteins and antibodies on a cellulose nanofibril film. Alternatively, a variety of other amine-containing entities could be coupled to carboxylates following a similar procedure. Even another crosslinker could be selected containing a new functionality in addition to the amine group. Thus, CNCs oxidized to CNC-COO^- and activated with NHS/EDC could be end-functionalized with thiol, maleimide or other groups necessary for intended application.

To conclude this literature review, various forms of cellulose can be applied to generate colloidal self-assembly. Cellulose is actively explored as a raw material for this purpose because of its renewability, biocompatibility and affordability. Most extensive attention has been paid on functionalization of cellulose surface hydroxyls to exaggerate the amphiphilicity of cellulose. As an alternative, selective functionalization of the reducing end of cellulose gathers interest, since this method can produce highly distinct anisotropy in the product. Furthermore, the native crystallinity of cellulose is more facile to retain while concentrating reactions at one end of the chain. These are substantial advantages compared to conventional cellulose modification techniques, which are often designed for applicability to cellulose derivatives. However, like surface hydroxyls, reducing ends frequently require activation to become sufficiently versatile to react with the intended compound. As potential activation methods, maleimide end-functionalization produces CNCs that are reactive with thiol groups from the reducing end, whereas thiol end-functionalization produces CNCs with highly versatile reactivity at the reducing end, including noble metal affinity and reactivity with maleimides.

3. Experimental

Materials and experimental methods used in this study are introduced in this chapter. Chemicals are specified in Section 3.1 and synthesis and measurement protocols in Section 3.2. An overview of the synthesis paths applied to obtain CNC-SH and CNC-MAL has been introduced in Chapter 1. Briefly, CNC reducing ends were thiol-functionalized via reductive amination or NHS/EDC-catalyzed coupling, as seen in Figure 1a. CNC-SH prepared via reductive amination was reacted with a homobifunctional maleimide crosslinker to yield CNC-MAL, as illustrated in Figure 1b. The thiolations were performed in water and the conversion of CNC-SH to CNC-MAL in ethanol. Sections 3.2.1 and 3.2.2 explain the thiolation methods in more detail, whereas Sections 3.2.3 and 3.2.4 present the developed protocol for CNC-MAL preparation. The analytical techniques, equipment and calculations employed for the characterization of the acquired samples are introduced in Sections 3.2.5, 3.2.6 and 3.2.7.

3.1 Chemicals

Hydrochloric acid (HCl) and diethyl ether were acquired from AnalaR Normapur and sodium bicarbonate from Merck. Dimethyl sulfoxide (DMSO) was purchased from Labscan, ethanol of technical quality from Altia and bismaleimide-poly(ethylene glycol) (BM-PEG, MW 1000) from Laysan Bio. Sigma-Aldrich supplied the other chemicals: sodium carbonate, 6-amino-1-hexanethiol hydrochloride (NH_2-R-SH), acetic acid, sodium triacetoxyborohydride, potassium chloride (KCl), Sodium chlorite ($NaClO_2$) *N*-hydroxysuccinimide (NHS), *N*-(3-Dimethylaminopropyl)-*N*′-ethylcarbodiimide hydrochloride (EDC), ethylenediaminetetraacetic acid (EDTA), monobasic sodium phosphate (NaH_2PO_4), pentaerythritol tetrakis(3-mercaptopropionate) (PTMP), 5,5'-dithiobis-(2-nitrobenzoic acid) (Ellman's reagent) and cysteine hydrochloride monohydrate. Spectra/por dialysis membrane (MWCO 6-8000) was obtained from Spectrum Laboratories and hardened ashless filter paper from Whatman. MilliQ water (MQ) was prepared with Synergy UV by Millipore.

3.2 Methods

3.2.1 CNC-SH Preparation via Reductive Amination

CNCs prepared via sulfuric acid hydrolysis of hardened ashless filter paper were end-functionalized with thiol groups via reductive amination as described previously (Lokanathan et al. 2013). In brief, CNC suspension (10 mg/ml, 50 ml) was buffered with 0.1 M carbonate buffer to pH 9.2 and placed in a water bath maintained at 70 °C. A total of 750 μmol NH_2-R-SH and 110 mmol sodium triacetoxyborohydride as a reducing agent were added in three steps over a period of 3 days accompanied by stirring (250 μmol NH_2-R-SH + 37 mmol reducing agent per day for 3 days). Between the first addition of NH_2-R-SH and the first addition of the reducing agent, 2.5 ml of 100% acetic acid was added. After three days the reaction mixture was cooled to room temperature, followed by adding 10 ml of 3 M HCl to neutralize the excess reducing agent. The neutralized reaction mixture was dialyzed against degassed MQ to remove the reducing agent, followed by addition of an appropriate amount of KCl salt to achieve a suspension including 2 M KCl. After stirring overnight, the suspension was again dialyzed against degassed MQ water to remove the electrolyte and unreacted NH_2-R-SH. The resulting thiol concentration was estimated to be 45.2±5 μmol per gram of CNC-SH, based on earlier measurements with this functionalization method (Lokanathan et al. 2013).

For optimization of the following conversion reaction, CNC-SH suspension in water was degassed by purging with nitrogen gas and stored airtight in a refrigerator without performing the following solvent exchange. For further experiments building on the optimized conversion, CNC-SH suspension was solvent exchanged from water to ethanol in order to prevent the degradation of the thiol and maleimide groups during further functionalization. The solvent was exchanged following a procedure described earlier (Kim et al. 2003). An equal amount of ethanol and CNC-SH suspension in water were mixed, and this mixture was evaporated to one-half its original volume. An equal amount of ethanol was added again, and the volume was re-evaporated to one-half. The ethanol addition and re-evaporation were repeated two more times to perform altogether four evaporations. The resulting CNC-SH suspension, with only ethanol remaining as a solvent, was stored airtight in a refrigerator before other experiments.

3.2.2 CNC-SH Preparation via NHS/EDC-Catalyzed Coupling

NHS/EDC-catalyzed coupling was selected as the alternative method for CNC-SH preparation because of its wide usage and relative simplicity. In contrast to reductive amination, NHS/EDC-catalysis targets carboxylates instead of aldehyde groups. Available carboxylates can be introduced at CNC reducing end via oxidation using $NaClO_2$ (Hieta, Kuga & Usuda 1984), whereas aldehydes only become available when terminal glucose rings open (slower, downward reaction in Figure 3). Thus, the overall reaction between CNC-COO^- and NH_2-R-SH catalyzed by NHS and EDC proceeds faster than the coupling of CNC and NH_2-R-SH via reductive amination. Furthermore, the elevated temperature of reductive amination is unnecessary. The reaction is based on the ability of a carboxylate group and NHS to form an ester in the presence of a carbodiimide, such as EDC (Hermanson 1996). Being a good leaving group, NHS can easily give way to an amine group, thus enabling the formation of a stable amide bond (Hermanson 1996).

A CNC suspension of 10 mg/ml was immersed in 250 mM $NaClO_2$ in MQ. After adjusting the pH to 3.5 with 50% acetic acid, the suspension was stirred at room temperature for 20 hours. The resulting CNC-COO^- suspension was purified via dialysis against MQ and diluted to 2 mg/ml. The diluted suspension was degassed and its pH adjusted to 7 before adding NHS. Right after NHS addition, EDC was added and pH restored to 6-7. After this, KCl and NH_2-R-SH were added and pH raised to 9.2 in varying order. The achieved concentrations and order of the chemicals added and pH adjustments made for each sample are displayed in Table 1.

All samples were incubated for two hours at room temperature and purified via dialysis against degassed MQ. As seen in Table 1, for samples Low EDC, Amine First and High pH, the dialysis was repeated again after stirring in 1 M KCl at room temperature overnight. For sample High Ion, steps 5 and 6 as well as first half an hour of the incubation step were performed in ultrasonicator bath in order to prevent CNC aggregation under increased ionic strength. All samples were degassed before storing airtight in a refrigerator before other experiments. Sample Low EDC was degassed and refrigerated airtight already after step 7. The incubation in KCl was implemented only after first QCM-D measurements on this sample.

Table 1: Different sample preparation protocols used for CNC thiolation via NHS/EDC-catalyzed coupling. Varying events are presented in bold.

Low EDC	**Amine First**	**High pH**	**High Ion**
1. 5 µM NHS	1. 5 µM NHS	1. 5 µM NHS	1. 5 µM NHS
2. 2 µM EDC	**2. 50 µM EDC**	**2. 50 µM EDC**	**2. 50 µM EDC**
3. pH to 6-7	**3. pH to 6-7**	**3. pH to 9.2**	**3. pH to 6-7**
4. 1 µM NH_2-R-SH	**4. 1 µM NH_2-R-SH**	**4. 1 µM NH_2-R-SH**	**4. ~1 M KCl**
5. **pH to 9.2**	**5. pH to 9.2**	5. Degassing and incubation	**5. 1 µM NH_2-R-SH**
6. Degassing and incubation	6. Degassing and incubation	6. Dialysis for excess reagents	**6. pH to 9.2**
7. Dialysis for excess reagents	7. Dialysis for excess reagents	**7. ~1 M KCl**	7. Incubation
8. ~1 M KCl	**8. ~1 M KCl**	8. Dialysis for KCl	8. Dialysis for excess reagents and KCl
9. Dialysis for KCl	9. Dialysis for KCl		

3.2.3 Optimization of the Conversion of CNC-SH to CNC-MAL in Water

For the conversion reaction, bismaleimide-poly(ethylene glycol) (BM-PEG) was selected as the necessary crosslinker because of its long poly(ethylene glycol) arm between the end maleimides. This spacer arm was expected to sterically force the maleimide in the further end beyond the spacer to remain unreacted. To further enhance this steric protection effect by also crowding out the reactive sites, BM-PEG was used in 50-fold molar excess compared to the estimated thiol concentration of CNC-SH.

Table 2: Addition of BM-PEG reagent solution to different CNC-SH suspensions and the resulting molar ratios of BM-PEG to thiols.

Sample	**Amount of BM-PEG added**	**Resulting BM-PEG:thiol molar ratio**
10c	40 µmol	10:1
50c	200 µmol	50:1
100c	400 µmol	100:1
0c	-	0:1

CNC-SH suspension in water was diluted to 2 mg/ml (thiol concentration approximately 90 µM) and buffered (85 mM NaH_2PO_4, 27 mM EDTA, pH 7). The acquired suspension was divided into four 50 ml samples referred to as 10c, 50c, 100c and 0c. BM-PEG dissolved in a small amount of DMSO was added to the sample suspensions to acquire BM-PEG to thiol molar ratios presented in Table 2.

Presented molar ratios of BM-PEG to thiol groups are estimated assuming the thiol concentration of CNC-SH to be 40 µmol/g. All samples were sonicated for 10 minutes

and stirred for 24 hours at room temperature, samples 10c, 50c and 100c covered in aluminium foil. After the incubation, samples were purified via dialysis against degassed MQ, degassed by purging with nitrogen gas and refrigerated in airtight containers.

3.2.4 Conversion of CNC-SH to CNC-MAL in Ethanol

The solvent-exchanged CNC-SH suspension was diluted with ethanol to 2 mg/ml (thiol concentration approximately 90 μM). After pH adjustment to 7, 50 ml of the suspension was mixed with 0.2 g (0.2 mmol) of BM-PEG dissolved in approximately 1 ml of ethanol. The pH-adjusted suspension with CNC-SH and BM-PEG was sonicated for 10 min and stirred for 24 hours at room temperature, covered in aluminum foil. Excess BM-PEG was removed by precipitating the CNCs from the solution by adding 15 ml diethyl ether. The precipitate was collected via centrifugation at 10 000 rpm for 30 min and redispersed in ethanol-diethyl ether (3:1) mixture. The redispersed mixture was again centrifuged to collect the precipitate. The redispersion and centrifugation were repeated two more times to perform altogether four centrifugations and three redispersions. After the final centrifugation, the precipitate was dispersed in ethanol and refrigerated in an airtight container. For comparison, a control sample was prepared via similar procedure without adding the BM-PEG.

3.2.5 Quartz-Crystal Microbalance with Dissipation (QCM-D)

QCM-D was used in this thesis to detect the presence of thiol or maleimide groups in CNCs by observing CNC adsorbance on surfaces. CNC-SH adsorbance was studied on a plain gold surface. For maleimide detection in CNC-MAL, a gold surface was first coated with PTMP. PTMP self-assembles on gold into monolayers with certain thiols bound to the gold and the other thiols accessible on the surface (Vercelli & Zotti 2007). These accessible thiols were expected to serve as attachment sites for CNC-MAL because of the specific reactivity between maleimide and thiol groups.

QCM-D is based on a piezoelectric quartz crystal placed between a working electrode and a counter electrode. This crystal, along with the attached electrodes, vibrates at a specific frequency and amplitude when exposed to a sinusoidal voltage. The energy of the oscillating voltage is most efficiently converted to energy of the vibration at the

resonant frequency of the crystal and electrode system. This resonant frequency changes when the mass of the system changes upon particle deposition (i.e., adlayer formation) or removal at the electrode-solvent interface. Thus, the frequency change (Δf) provides qualitative and quantitative information about the adsorption processes occurring on the working electrode.

A QCM-D device also measures the amplitude of the crystal oscillation. The crystal can almost completely transform the electrical energy from the voltage source into its own vibration as long as it has no or only a rigid adlayer. Thus, even without continuous energy addition, it can sustain the same amplitude over an extended period of time. Conversely, a crystal with a flexible adlayer will dampen the oscillation. If additional electrical energy is not continuously applied, the amplitude will decrease over time. This energy dissipation is also recorded by the device. Data about the dissipation change (ΔD) provides information about the viscoelastic qualities of the adsorbed samples.

In this thesis, the resonant frequency and the dissipation were recorded using QCM-D E4 instrument and gold-covered quartz crystals purchased from Q-Sense, a flow rate of 0.1 ml/min and a temperature of 23 ^{o}C. Before the measurement, the crystals were first cleaned by UV/ozone treatment for 30 min, followed by sonication in acetone for 30 min. The cleaned crystals were dried with nitrogen gas and placed in QCM-D chambers for the adsorption studies of CNC-SH samples. In the case of CNC-MAL and its control samples, the cleaned crystals were first functionalized with thiol groups by immersing them in 1 mM solution of PTMP in ethanol for 30 min. Physisorbed or loosely bound PTMP molecules were removed by sonicating the crystals in ethanol for 30 min. The thiol-covered crystals were placed in QCM-D chambers after drying with nitrogen gas.

Before the measurements, all samples were sonicated for 30 min and diluted to 1 mg/ml or 0.1 mg/ml. The samples suspended in ethanol (i.e., CNC-MAL and its control) were solvent exchanged with degassed MQ prior to the dilution. The solvent was exchanged as described in Section 3.2.1, with only three rounds of evaporations and water additions because ethanol and residues of diethyl ether are removed faster than water.

Before exposure to the sample suspensions, the chambers were first rinsed with degassed MQ to establish a stable baseline signal for the resonant frequency and dissipation signals. After approximately eight minutes of stable baseline, the sample suspensions were flowed through the chambers. Finally, potential reversibly adsorbed sample was rinsed off with degassed MQ.

Overtones 1, 3, 5, 7, 9, 11 and 13 of the resonant frequency of the crystal were recorded. The results analyzed further and presented in Section 4.1 are based on the 7^{th} overtone. In other words, the 7-fold resonant frequency of the quartz crystal and the dissipation of the oscillation at this frequency are compared to those of the plain crystal immersed in baseline water. Thus, the change in this overtone of the resonant frequency and dissipation are recorded.

3.2.6 Atomic Force Microscopy (AFM)

AFM was used in order to directly visualize the adsorbed CNC-MAL on the QCM-D crystal surface. After QCM-D measurements, the crystals with CNC-MAL were dried with nitrogen gas and imaged with AFM. The placement of the individual CNC-MALs on the crystal surface was expected to provide further information about the behavior of CNC-MAL when attaching on a thiol-covered surface.

AFM images the topographies and morphologies of sample surfaces by moving a small tip along the surface. The tip is attached to a cantilever that, depending on the operation mode of the AFM, either bends (contact mode) or changes its oscillation amplitude (non-contact or tapping mode) according to the interactions with the surface structures. The bending or oscillation change can be measured by observing the movement of a laser beam reflected from the back of the cantilever to a quadrant photodetector.

In this thesis, AFM images were recorded in air using a Nanoscope IIIa multimode scanning probe microscope with scanner E manufactured by Digital Instruments. The AFM was operated in tapping mode, using silicon cantilevers (force constant 46 N/m, resonance frequency 325 kHz) supplied by µmash. Images were recorded from five varying spots per sample and flattened using NanoScope software (version 8.15, Bruker).

3.2.7 Ellman's Assay

Ellman's assay utilizes the reactivity of Ellman's reagent towards thiol groups as presented in Figure 5. Unlike Ellman's reagent, its cleaved form TNB has a UV light absorption peak at a wavelength of 412 nm. Therefore, a thiol-containing sample incubated in the presence of Ellman's reagent absorbs more UV light at this wavelength than a similarly prepared sample with no thiols. This is caused by the cleavage of Ellman's reagent to TNB in the thiol-containing sample. Thiol concentration in a sample directly correlates with the UV absorption measured in it at a 412-nm wavelength (Hermanson 1996).

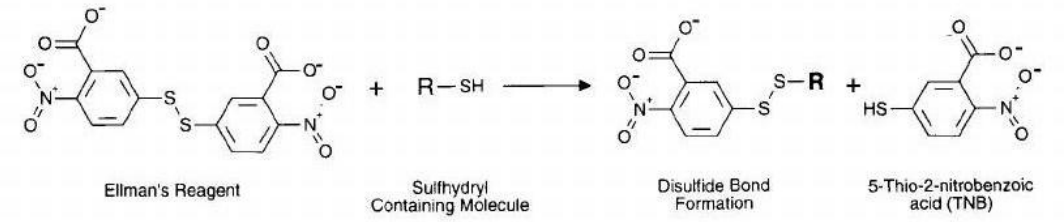

Figure 5: The cleavage of Ellman's reagent in the presence of sulfhydryl (thiol) groups (Hermanson 1996).

On CNC-SH, this assay was applied in order to directly quantify the amount of thiol groups present in the final samples. In the case of optimizing conversion of CNC-SH into CNC-MAL, Ellman's assay served as a method for quantification of the thiol groups remaining in CNCs before and after the conversion reaction. In addition, to enable maleimide quantification, the assay provided information about cysteine molecules remaining in a CNC-MAL sample after incubation with an excess of cysteine. In preparation for the assay, suspensions were prepared of each sample in buffer (0.1 mM NaH_2PO_4, 1 mM EDTA, pH 8) according to Table 3. In addition, to enable quantification of the introduced groups, a series of cysteine standard solutions was prepared as described in Appendix.

Each sample suspension and blank solution was mixed with 50 µl of Ellman's reagent solution prepared by dissolving 4 mg of Ellman's reagent into 1 ml of similar buffer. After a 15-min incubation, the absorbance of each mixture for UV light at a wavelength of 412 nm was measured with UV-2550 UV-Vis Spectrophotometer (Shimadzu). From the acquired value, the corresponding value for a blank solution was subtracted (*Blank*

with EtOH from ethanol-containing samples or *Blank* from others). Respectively, corresponding baseline solutions were used to reset the device before measuring. The measurements were repeated twice for samples Low EDC, Amine First, High pH and High Ion; three times for samples 10c, 50c, 100c and 0c and twice for samples CNC−MAL and CNC‑MAL + cys. For CNC‑SH, two repetitions were performed with ethanol and three repetitions without.

Table 3: Sample compilations for Ellman's assay.

	Sample name	**CNC sample concentration**	**EtOH : buffer**	**Cysteine**
CNC-SH via NHS/EDC-catalyzed coupling	Low EDC	0.5 mg/ml	-	-
	Amine First	0.5 mg/ml	-	-
	High pH	0.5 mg/ml	-	-
	High Ion	0.5 mg/ml	-	-
CNC-MAL optimization	10c	0.5 mg/ml	-	-
	50c	0.5 mg/ml	-	-
	100c	0.5 mg/ml	-	-
	0c	0.5 mg/ml	-	-
	Blank	-	-	-
	Baseline	-	-	-
	CNC-MAL	0.5 mg/ml	1:2	-
	CNC-MAL + cys	0.5 mg/ml	1:2	50 µM
	Blank with EtOH	-	1:2	-
	Baseline with EtOH	-	1:2	-
	CNC-SH via reductive amination	0.5 mg/ml	1:2 (2 rep.) or none (3 rep.)	

The ratio between the thiol concentration and UV absorbance can be determined by plotting the absorbance values of the cysteine standard solutions. Assuming a similar ratio for varying thiol samples, the thiol concentration c_{SH} is determined by equation

$$c_{SH} = \frac{A_{SH}}{\Delta A_{cys} / \Delta c_{cys}}, \quad (1)$$

where A_{SH} is UV absorbance caused by thiols

$\Delta A_{cys}/\Delta c_{cys}$ is slope of the cysteine standard plot (μM^{-1}).

When estimating the thiol concentration of CNC-SH, the absorbance value of a pristine CNC sample needs to be subtracted from that of CNC-SH in order to determine the absorbance caused by thiols. This is due to the CNC particles scattering the UV light, thus affecting the measured absorbance. For maleimide concentration c_{MAL} estimation, the UV absorbance caused by thiols corresponds to the difference between the absorbances in samples CNC-MAL and CNC-MAL + cys, according to equation

$$A_{SH} = A_{CNC\text{-}MAL+cys} - A_{CNC\text{-}MAL}, \quad (2)$$

where $A_{CNC\text{-}MAL+cys}$ is absorbance by CNC-MAL + cys

$A_{CNC\text{-}MAL}$ is absorbance by CNC-MAL.

Knowing the concentration of cysteine added to CNC-MAL + cys in order to achieve an excess of cysteine available for reacting with the maleimides present, maleimide concentration in the sample is determined by equation

$$c_{MAL} = c_{cys} - c_{SH}, \quad (3)$$

where c_{cys} is original concentration of cysteine (μM)

c_{SH} is concentration of thiols after incubation (μM)

Combining equations (1), (2) and (3), the maleimide concentration in sample CNC-MAL can be calculated from the equation

$$c_{MAL} = c_{cys} - \frac{A_{CNC-MAL+cys} - A_{CNC-MAL}}{\Delta A_{cys} / \Delta c_{cys}}. \quad (4)$$

4. Results

This chapter presents the results of the experiments described above in Chapter 3. The chapter is divided into sections based on the measurement techniques used to acquire the results. QCM-D data are introduced in Section 4.1, AFM images in Section 4.2 and the results from Ellman's assay in Section 4.3.

4.1 Quartz-Crystal Microbalance with Dissipation

The adsorption of CNC-SH suspensions (0.1 mg/ml) on gold was studied with QCM-D, as introduced in Section 3.2.5. For sample Low EDC, QCM-D micrograph was recorded twice: before and after incubation in KCl. For the other three samples, QCM-D measurements were performed once, at the end of the whole synthesis. The QCM-D micrographs of resonant frequency change (Δf) and dissipation change (ΔD) for sample Low EDC before and after incubation in KCl are presented in Figure 6. In this figure, a clear decrease in resonant frequency and increase in dissipation can be observed after introducing CNC-SH that has not been treated with KCl. In contrast, no change occurs in either when introducing KCl-treated CNC-SH. The contrast in frequency changes noticeable in Figure 6a implies that the Low EDC sample is adsorbing on gold before but not after treatment with KCl. The high dissipation change observed for the non-KCl-treated sample in Figure 6b suggests that the adsorbance occurs as a flexible layer.

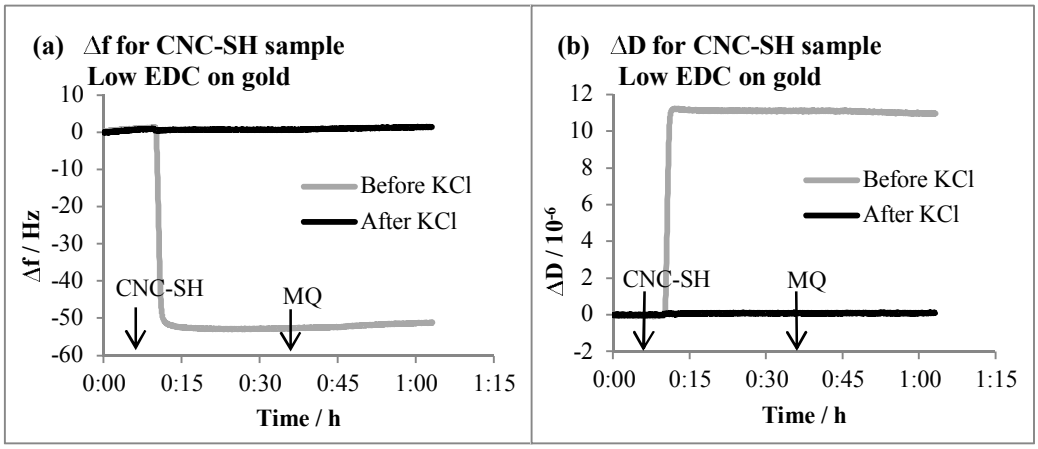

Figure 6: QCM-D micrographs (7th overtone) for CNC-SH sample Low EDC on gold, both before and after incubation in KCl.

The resonant frequency and dissipation graphs for other CNC-SH samples on gold are displayed in Figure 7. Based on Figure 7a, samples Amine First and High pH apparently adsorb on gold to a limited extent, achieving only a frequency change of approximately -5 Hz. Nevertheless, sample High Ion appears to possess a higher affinity towards gold, changing the resonant frequency with more than -35 Hz. Therefore, sample High Ion probably contains more introduced thiol groups than the other CNC-SH samples. According to Figure 7b, the adsorption of sample High Ion also increases the dissipation by approximately $2.5 \cdot 10^{-6}$. Therefore, this sample probably adsorbs as a flexible layer. However, neither frequency nor dissipation change achieves the level of those attained by sample Low EDC before KCl.

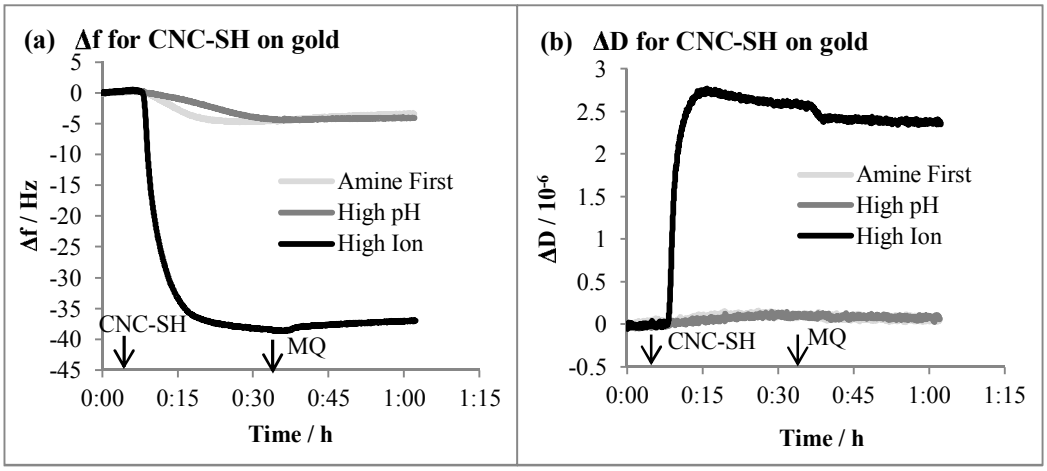

Figure 7: QCM-D micrographs (7th overtone) of different CNC-SH samples on gold. Graphs for samples Amine First and High pH partly overlap.

Based on the data presented in Figure 6 and Figure 7, ΔD values of various CNC-SH samples are plotted against their respective Δf values in Figure 8. The plots have linear sections with slopes of $-0.22 \cdot 10^{-6}$ Hz^{-1} for sample Low EDC before KCl (R^2 = 0.998); $-0.10 \cdot 10^{-6}$ Hz^{-1} for sample High Ion (R^2 = 0.9886) and $-0.02 \cdot 10^{-6}$ Hz^{-1} for samples Amine First and High pH. These results show that the sample without a KCl treatment produces the most viscoelastic adlayer. In contrast, the samples with least adsorption (i.e., Amine First and High pH), also adsorb in the most rigid formation.

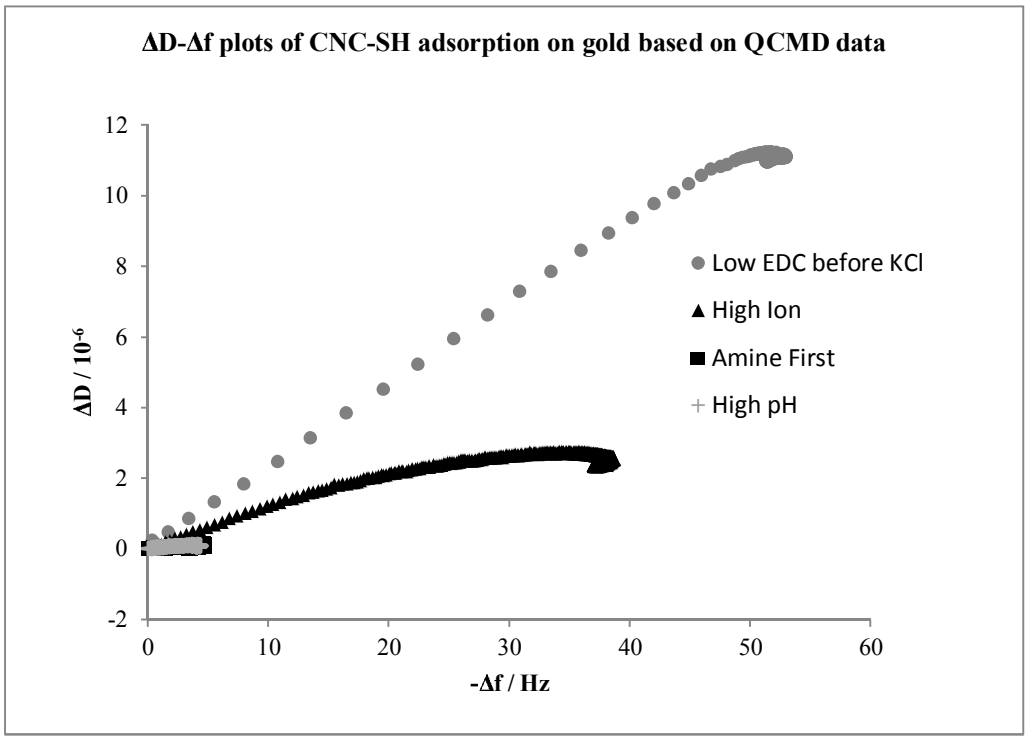

Figure 8: ΔD-Δf plots representing the adsorption of different CNC-SH samples on gold between 6 min and 1 hour. Plots for samples Amine First and High pH overlap.

The presence of maleimide in CNC-MAL was verified by examining the ability of CNC-MAL to adsorb on a gold surface covered with PTMP, as explained in detail in Section 3.2.5. The results of this experiment are presented in Figure 9. Figure 9a expresses that the resonance frequency of the thiol-covered QCM-D crystals decreases after exposure to CNC-MAL. Since the decrease in resonance frequency corresponds to increase in the crystal mass, this implies that CNC-MAL includes maleimide groups that react with the surface thiols and thus cause CNC-MAL to adsorb on the surface. This adsorption appears to take place faster and to a greater extent with increased CNC-MAL concentration because the resonance frequency plot of CNC-MAL with 1 mg/ml decreases earlier and further than that with 0.1 mg/ml. However, this adsorption is far smaller than that of the most adsorbing CNC-SH samples. CNC-MAL adsorption resembles more closely that of CNC-SH samples Amine First and High pH.

As seen in Figure 9b, the dissipation follows a similar pattern to resonant frequency upon CNC-MAL exposure, only towards the opposite direction. After the CNC-MAL

introduction, the dissipation of the crystals increases, suggesting adsorption of an at least slightly viscous layer. Similar to frequency change, the dissipation increase appears less noticeable for CNC-MAL than CNC-SH samples Low EDC before KCl and High Ion. Nevertheless, CNC-MAL adsorption appears to dissipate crystal oscillation more than the less adsorbing CNC-SH samples. Since these samples adsorb in approximately similar amounts with CNC-MAL, a CNC-MAL adlayer is probably more viscoelastic than that of the less dissipating CNC-SH adlayers.

This expectation is confirmed by the plots depicted in Figure 9c. According to this figure, dissipation changes almost linearly with resonant frequency for both concentrations of CNC-MAL. The ΔD-Δf plots have slopes of $-0.09 \cdot 10^{-6}$ Hz^{-1} for 1 mg/ml CNC-MAL ($R^2 = 0.9925$) and $-0.05 \cdot 10^{-6}$ Hz^{-1} for 0.1 mg/ml CNC-MAL ($R^2 = 0.9471$). These slope values, particularly the value obtained with the more concentrated sample solution, appear fairly similar to the same value for the CNC–SH sample High Ion. Based on this comparison, CNC-MAL can be expected to adsorb on PTMP-covered gold in a more limited amount but in an as flexible arrangement as CNC-SH High Ion on plain gold.

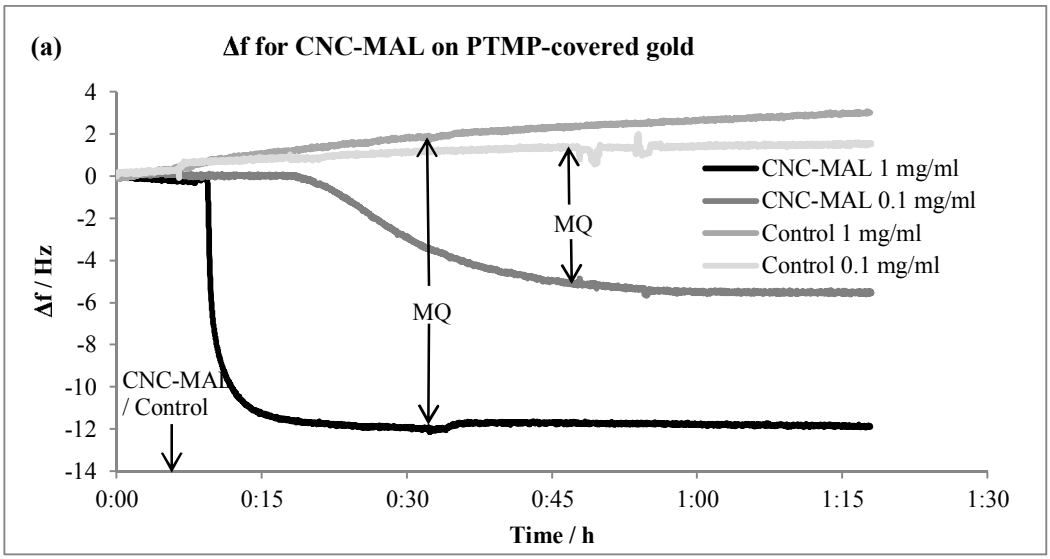

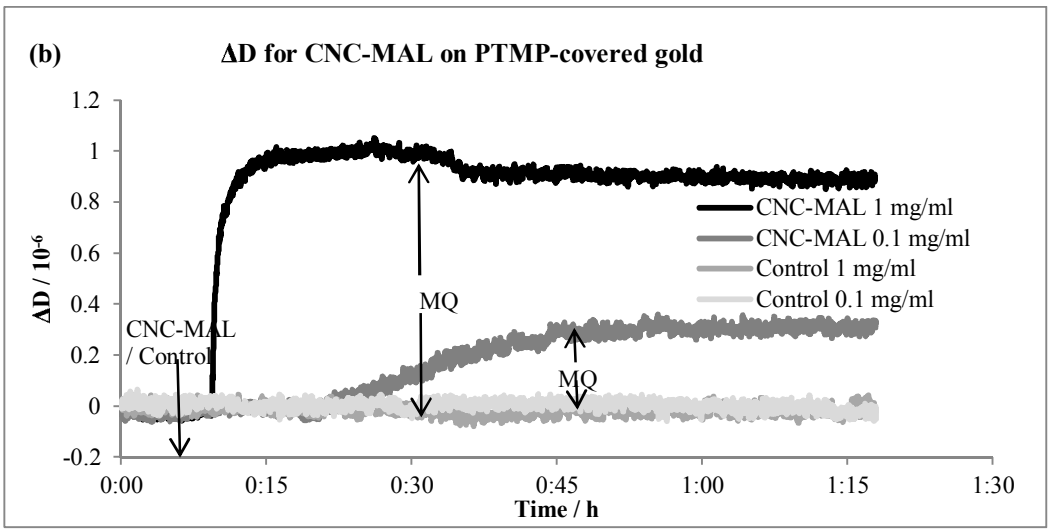

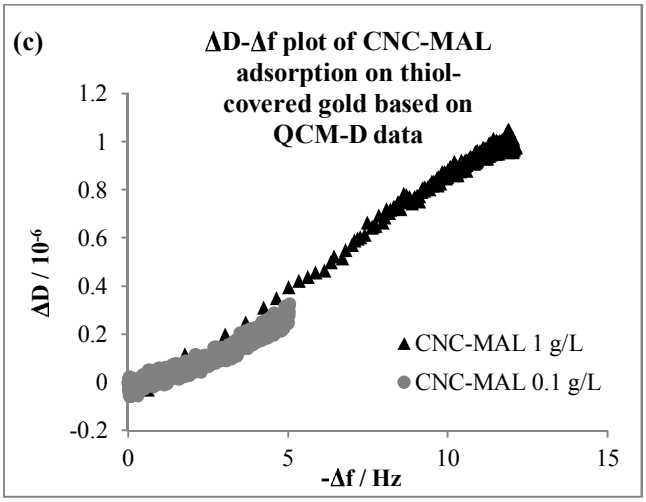

Figure 9: QCM-D data (7th overtone) of the adsorption of CNC-MAL and control suspensions on PTMP -covered gold:

Changes in (a) resonant frequency and (b) dissipation (controls overlap) plotted over time with CNC-MAL or control suspension introduced at 8 min and MQ at 33 min to 1 mg/ml samples or at 48 min to 0.1 mg/ml samples

(c) Dissipation - frequency response upon adsorption plotted between 7 min and 33 min for 1 mg/ml CNC-MAL and between 7 min and 48 min for 0.1 mg/ml CNC-MAL

4.2 Atomic Force Microscopy

The recorded AFM images are presented in Figure 10. With both concentrations of CNC-MAL, the QCM-D crystal surfaces seem fairly smooth, without the expected white rod-like shapes representing CNCs. Considering the results suggesting limited adsorption of CNC-MAL in QCM-D (Section 4.1), this could be due to long distances between the individual CNC-MAL rods decreasing the probability of the imaged areas containing even one of them.

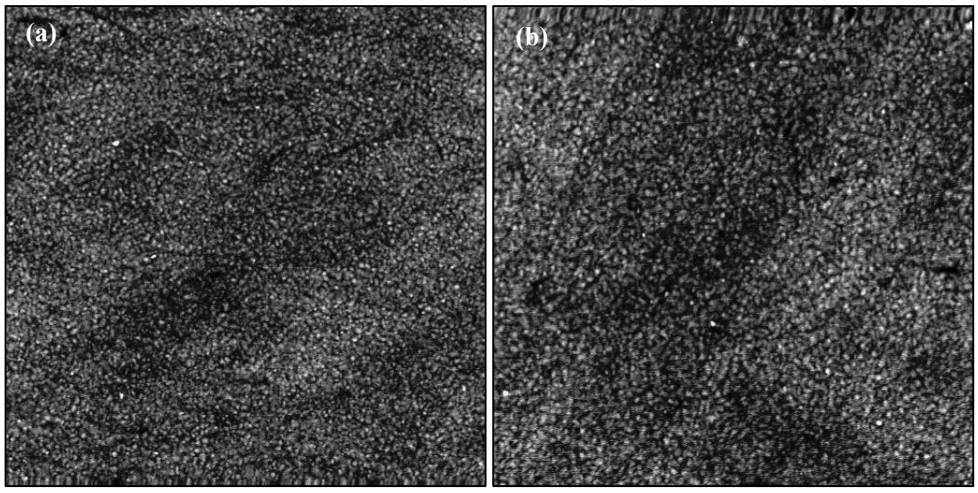

Figure 10: AFM height images of thiol-covered gold surface after QCM-D experiments with CNC-MAL in concentrations (a) 0.1 mg/ml and (b) 1 mg/ml. Image sizes are (a) 5 µm x 5 µm and (b) 4.51 µm x 4.51 µm.

4.3 Ellman's Assay

For CNC-SH prepared via NHS/EDC-catalyzed coupling, no adsorption peak at 412 nm was observed with Ellman's assay. That is why here are presented only the results used to optimize CNC-SH to CNC-MAL conversion and to quantify the maleimide concentration of CNC-MAL.

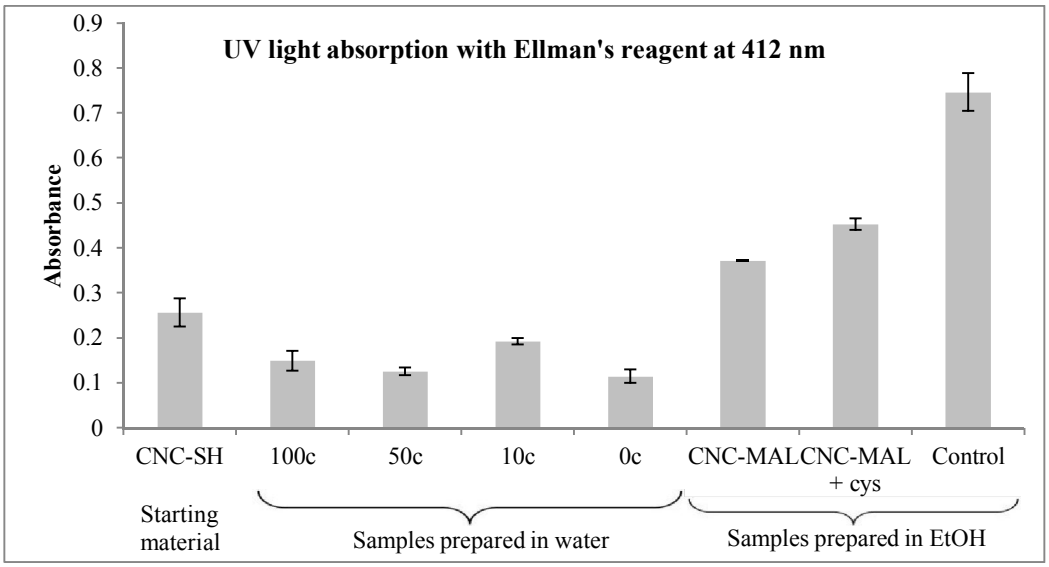

Figure 11: UV light absorption of CNC-MAL and control samples and their starting material incubated with Ellman's reagent.

Figure 11 presents the extent to which the different CNC-MAL and control samples (Sections 3.2.3 and 3.2.4) and their starting material CNC-SH (Section 3.2.1) absorb UV light at a wavelength of 412 nm. Since the absorption peak at this wavelength is caused by a form of Ellman's reagent that has been cleaved in a reaction with a thiol group, the measured absorption value corresponds to the thiol concentration of the sample. The high absorbance of the starting material sample (CNC-SH prepared via reductive amination) implies that the reductive amination (Section 3.2.1.) was successful at introducing thiol groups in the CNCs in preparation for maleimide conversion. All the other samples, which have completed a 24-hour incubation with varying amounts or even none of BM-PEG, absorb less. In the case of samples 100c, 50c and 10c, part of this absorption decrease assumedly results from the thiols of CNC-SH reacting with the maleimide groups of BM−PEG.

As displayed in Figure 11, lowest absorption corresponding to smallest thiol concentration occurs in samples 50c and 0c. In comparison to samples 10c and 100c, the low absorption of sample 50c suggests that the 50-fold concentration of BM‑PEG in relation to thiols has probably converted more thiols to maleimide than the higher and lower BM‑PEG concentrations. Therefore, a molar ratio of 50:1 between the maleimide

reagent and the existing thiol groups in CNC-SH can be interpreted to produce the highest yield of thiol conversion to maleimide.

However, even sample 0c with no exposure to BM-PEG absorbs approximately as little as the sample 50c. This indicates that a significant amount of thiol groups spontaneously degraded during incubation. During the actual conversion of CNC-SH to CNC-MAL following the optimized protocol, this thiol degradation was suppressed by utilizing an organic solvent. The effect of the solvent seems significant based on Figure 11. The control sample, which has been solvent exchanged from water to ethanol after the reductive amination, absorbs about three times more UV light at 412 nm than sample CNC-SH, which has been stored airtight in degassed MQ and refrigerator over the week that has passed while preparing the CNC-MAL samples. This corresponds to the degradation of one third of the thiols in CNC-SH during a week-long storage.

From CNC-MAL to CNC-MAL + cys, an increase in adsorption is expected because of the thiols in the added cysteine. According to Figure 13 in Appendix, the 50 µM of cysteine added in this experiment causes an absorption between 0.09 and 0.57. As suggested by Figure 11, the absorbance actually increases from CNC-MAL to CNC-MAL + cys by 0.08±0.01. Even though the minimum of the standard and maximum of the experiment overlap, most likely the absorption increases from CNC-MAL to CNC-MAL + cys with less than the contribution of the added cysteine. This implies that CNC-MAL includes maleimide that is able to consume excess cysteine by reacting with it.

The maleimide concentration of CNC-MAL was calculated by inserting to equation (4) the measured absorbance values for CNC-MAL and CNC-MAL + cys; the added concentration of cysteine in CNC-MAL + cys (Section 3.2.7) and the slope of the cysteine standard plot (Appendix). Thus, CNC-MAL was estimated to contain 57.6±23.3 µmol of maleimide per gram of dry sample. This high maleimide content is unexpected due to the estimated thiol concentration of only 45.2±5 µmol/g in the CNC-SH used to prepare the CNC-MAL (Section 3.2.1). Nevertheless, taking the error into account, CNC-MAL may even include as little maleimide as 34.3 µmol/g.

5. Discussion

In this chapter, the results presented in Chapter 4 are evaluated in comparison to relevant literature presented in Chapter 2. The success of the thiol end-functionalization of CNCs via NHS/EDC-catalyzed coupling is evaluated in Section 5.1, whereas Section 5.2 assesses the achievement of the conversion of introduced end thiols into maleimides. Suggestions for future research are provided in Section 5.3.

5.1 CNC-SH Preparation via NHS/EDC-Catalyzed Coupling

The adsorption studies performed on sample Low EDC, both before and after incubation in KCl salt solution, highlight the importance of increasing the ionic strength during the CNC−SH preparation. Under low ionic strength (sample Low EDC before KCl), the NH_2−R−SH apparently adsorbs on CNC surface electrostatically. The high ionic strength (sample Low EDC after KCl) screens the negative charge of the CNC surface and the positive charge of the amine group in NH_2−R−SH (dominant when pH under 9.2), thus releasing the electrostatically adsorbed NH_2−R−SH. An incubation step under high ionic strength has also been included as an essential part of the development of CNC end-thiolation via reductive amination (Lokanathan et al. 2013).

For other CNC-SH samples, incubation in high ionic strength was performed before QCM−D measurements. Comparison of these samples to Low EDC after KCl shows that EDC:NHS molar ratio of 10:1 is more effective than the lower ratio of 2:5 for reacting the carboxylates of CNC−COO^- with the amine of NH_2−R−SH. Even sample Amine First, which is prepared following otherwise exactly the same protocol with Low EDC except for the increased EDC:NHS ratio, adsorbs on gold more than Low EDC after KCl. Previous studies involving NHS/EDC-catalysis have applied various EDC:NHS molar ratios, including 5:1 (Pieper et al. 2000), 1:1 (Araki, Kuga & Magoshi 2002, Bentzen et al. 2005), 1:4 (Orelma et al. 2012) and 1:16 (Jiang et al. 2004). Additional experiments with varying ratios would probably be required to discover the optimal composition for this reaction.

Comparison among the samples prepared using the more effective EDC:NHS ratio suggests that the protocol implementing the increase in ionic strength right after adding NHS and EDC to the starting material, before introducing NH_2−R−SH or raising pH, produces CNC-SH with the highest thiol content. Apparently, maintaining the negative charge of the CNC surface screened during exposure to NH_2−R−SH is the most effective way to direct the amines to react with the NHS/EDC-activated carboxylates in the reducing end. Distinctly smaller thiol-functionalization is achieved even when conducting the NH_2−R−SH addition in high pH to maintain the amine groups in their neutral, deprotonated form. The limited thiol content of sample High pH may be due to the accelerated degradation of NHS esters in basic conditions. Already at pH 8.6, the half-life of an NHS ester has decreased to 10 min (Hermanson 1996). Therefore, even though the NH_2−R−SH would exist in its uncharged form, there might be few NHS/EDC-activated carboxylates left for them to react with.

Based on the ΔD-Δf plot (Figure 8), the viscoelastic properties of the High Ion adlayer resemble those of an adlayer of CNC-SH prepared via reductive amination (Lokanathan et al. 2013). The relatively steep ΔD-Δf slope ($-0.10 \cdot 10^{-6}$ Hz^{-1}) indicates that the CNC-SHs prepared via NHS/EDC-catalyzed coupling under high ionic strength are adsorbing in an upright orientation with the end thiol attached to the gold surface and the CNC rod pointing outwards and free to move. In contrast, samples Amine First and High pH adsorb with a remarkably smaller ΔD-Δf slope of $-0.02 \cdot 10^{-6}$ Hz^{-1}, probably due to these CNC-SHs only adsorbing occasionally and in a flat orientation. The flat adsorption might result from the individual CNC-SHs being so separated that their interactions are insufficient for maintaining the CNC rods upright. Moreover, these samples might contain so few thiols that a major part of the occasional adsorption is caused by a very weak interaction between gold and the CNC surface.

In comparison to Amine First, High pH and even the more viscoelastic High Ion adlayers, the ΔD-Δf slope for sample Low EDC before KCl is extremely steep. Therefore, this sample probably produces a particularly flexible adlayer. However, this adsorption is assumedly caused by thiols in electrostatically adsorbed NH_2-R-SH, since the adsorption on gold ceases after the incubation of this sample under high ionic

strength. These thiols are located on the CNC surface and thus inclined to facilitate flat adsorption. Therefore, sample Low EDC before KCl possibly adsorbs in several layers, which might contain water, thus constructing a heavy and viscoelastic adlayer.

Multilayers of CNCs have been constructed in QCM-D before by adsorbing layers of cationized nanofibrillated cellulose in between to facilitate electrostatic attraction of new CNC layers (Olszewska et al. 2013). In this study, frequency decreases between few dozens and close to two hundred were measured for these multilayers. In contrast, in this thesis, NH_2-R-SH acts as the cationic mediator. Being remarkably smaller than a cellulose nanofibril, this molecule naturally causes a less prominent decrease in resonant frequency. Nevertheless, the ΔD-Δf slope acquired here ($-0.22 \cdot 10^{-6}$ Hz^{-1}) is even steeper than the slope obtained with multilayers of CNCs and cellulose nanofibrils (approximately $-0.15 \cdot 10^{-6}$ Hz^{-1}) (Olszewska et al. 2013). This could result from the CNC adlayer of this thesis being close to as highly dissipative but clearly lighter in mass compared to the mixed nanocellulose multilayer examined earlier.

In addition to QCM-D, the introduction of thiol groups to CNC reducing ends was confirmed with X-ray photoelectron spectroscopy and transmission electron microscopy (data not shown).

5.2 Conversion of CNC-SH to CNC-MAL

Comparing the QCM-D results (Section 4.1) to a previous study (Lokanathan et al. 2013), even for the better performing concentration of 1 mg/ml CNC−MAL, the frequency decreases far less than for CNC-SH prepared similarly to the reductive amination protocol applied in this thesis (Section 3.2.1). These authors measured frequency decreases of close to 40 Hz with CNC−SH concentrations of both 1 mg/ml and 0.1 mg/ml. This difference is unlikely to result from the mass of the individual adsorbate particles because both CNC−MAL and CNC−SH primarily consist of similar CNC. Therefore, CNC−MAL can be presumed to have only adsorbed in a very small quantity. The dissipation increase is, for 1 mg/ml CNC−MAL, less than one third, and for 0.1 mg/ml CNC−MAL, less than one tenth of that achieved in the corresponding earlier study (Lokanathan et al. 2013). Due to the viscoelastic similarity between

CNC−MAL and CNC−SH, this difference is also more likely due to poor adsorption than rigidity of the adsorbed layer.

The limited adsorption might be caused by a poor yield of CNC−SH conversion to CNC−MAL, possibly due to thiol and/or maleimide degradation before and/or during maleimide conversion or self-coupling between CNC−SH via BM−PEG bridges. Evidence for thiol degradation is presented more in detail in Section 4.3. Self-coupling is expected to remain under control when using a large excess of the crosslinker (Lowe 2010). However, it could be further inhibited by adding CNC−SH suspension more slowly to BM−PEG solution in the beginning of the conversion (Li et al. 2010a). Moreover, even if a considerable yield of CNC‑MAL was initially obtained, the introduced maleimide groups remain susceptible to hydrolysis, yielding maleamic acid, which lacks the thiol reactivity (Hermanson 1996). Comparing the QCM‑D results to the maleimide quantification presented in Section 4.3, though, it is unlikely that the poor adsorption originates solely from limited presence of maleimide groups. Possible other contributions to the adsorption results could be assessed by more precisely examining the ability of CNC-MAL to react properly with PTMP in the QCM‑D chamber conditions.

Following the trend of the absolute changes in resonant frequency and dissipation, also the ΔD-Δf slopes are less steep than measured earlier for similar concentrations of CNC−SH on gold (Lokanathan et al. 2013). This implies that CNC−MAL is a more rigid adsorbate than CNC−SH. Since individual CNC−MAL and CNC−SH particles have very similar structures, this is probably due to the CNC−MAL adsorbing in such a small quantity that individual particles are left far from each other. Not being surrounded by other particles, they probably fail to express the viscoelastic properties of a denser layer of functionalized CNCs.

The scattered arrangement of CNC-MAL on the crystal is underlined by the AFM images (Section 4.2) where, supposedly, CNC-MAL could not be visualized even when searching from five different 5 μm x 5 μm areas. However, based on QCM-D and AFM results attained earlier (Lokanathan et al. 2013),

approximately 3 particles / μm^2 would be expected for 0.1 mg/ml of CNC-MAL or 14 particles / μm^2 for the more concentrated CNC-MAL sample, assuming that the adsorbed particle densities linearly follow the QCM-D frequency decreases. These estimations would correspond to 75 CNC rods visible in Figure 10a and 285 in Figure 10b. Since these CNCs remain undiscovered, particle density probably fails to correlate with the QCM-D frequency decrease, possibly due to very uneven distribution of CNC-MAL on the PTMP-covered gold surface.

The results from Ellman's assay (Section 4.3) highlight the vulnerability of the thiol groups to oxidation and disulfide crosslinking, since part of them have apparently degraded while exposed to dissolved oxygen (Hermanson 1996). In the case of samples 100c, 50c and 10c, part of the thiol groups have assumedly disappeared due to their reaction with the maleimide groups in BM−PEG. This phenomenon appears the strongest in sample 50c. Therefore, 50:1 can be regarded as the most optimal molar ratio for BM-PEG and CNC-SH thiols. This ratio is very different from an earlier approach to measure a slight molar excess of thiols and proceed until complete consumption of the maleimide reagent (Pounder et al. 2008). However, these authors utilized significantly smaller thiol-containing units, which diffuse and react faster than the thiol moieties of CNC−SH. Considering this fundamental difference in the setting, it is still reasonable to assume that a large excess of maleimide is necessary for extensive conversion of CNC−SH to CNC−MAL.

The low absorption by sample 0c reveals that a high amount of thiol groups degrades from CNC−SH even when the starting material is incubated without the presence of a maleimide-containing reagent. This emphasizes the importance of carefully separating the CNC−SH from dissolved oxygen. An earlier study examined a 40-hour incubation of reduced proteins in 0.1 M neutral sodium phosphate buffer at 4 ^{o}C. Up to 90% or less than 7% of available thiol groups could be degraded without or in the presence of EDTA, respectively (Yoshitake et al. 1979). EDTA inhibits thiol degradation by chelating metal ions that catalyze thiol oxidation (Hermanson 1996). In this experiment, EDTA was used in buffers for both maleimide conversion in water and Ellman's assay. However, the UV absorption results imply that more than 7% of thiols have been lost.

Therefore, the thiol degradation in this experiment is probably less significantly influenced by the metal ion catalysis. In contrast, the utilized solvent appears to more strongly influence the thiol group stability, since solvent exchanging the CNC−SH from water to ethanol significantly suppressed the thiol degradation.

The deviation range of the estimated maleimide concentration (57.6±23.3 μmol/g) is unexpectedly wide. This estimation can include an error of up to 40%. Moreover, the middle and high end of the range are unrealistic because, assumedly, the starting material CNC-SH only contains 45.2±5 μmol/g of thiols. Nevertheless, the lower end of the range of the estimated maleimide concentration of CNC-MAL (34.3 μmol/g) corresponds to approximately 76% of the thiol groups in CNC−SH converted. This estimation is consistent with the previous result of 80% conversion of thiol end-functionalized polymer using a bismaleimide crosslinker (Li et al. 2010a). Therefore, the low end of the result range is most credible, considering that only a certain portion of the CNC‑SH thiol groups can be converted to maleimide groups.

Comparing the results obtained with QCM‑D (Section 4.1) and Ellman's assay (Section 4.3), both methods appear to qualitatively confirm that maleimide groups exist in CNC−MAL. Without maleimide groups, CNCs would not adsorb on thiol-covered gold as seen in Figure 9, and an addition of cysteine would cause a higher increase in UV absorbance than displayed in Figure 11. Quantitatively, however, QCM‑D suggests even less maleimide than the 34.3 μmol/g estimated by Ellman's assay. The lower expectation is based on comparing the poor CNC‑MAL adsorption on a thiol-covered surface to the previously measured CNC‑SH (45.2±5 μmol/g of thiols) adsorption on a gold surface (Lokanathan et al. 2013). Surprisingly high amount of maleimides might be observed with Ellman's assay if a large fraction of BM−PEG remains in CNC−MAL even after purification (Section 3.2.4). This kind of BM−PEG trace would, being a small molecule compared to CNC−MAL, affect little the QCM−D adsorption.

Based on the incompatibility with other results and the strong deviation in the calculated result, the reliability of Ellman's assay can be questioned as a malemide quantification method. An alternative quantification method would refer to the UV absorption peak of

maleimide itself at a wavelength of 300 nm (Hermanson 1996). For example, the absorbance of the CNC–SH mixed with BM–PEG could be measured before and after the 24-hour incubation to determine the absorbance lost because of the maleimides in BM–PEG consumed in the conversion reaction. Even though this method would not separate between BM–PEG reacting from one maleimide only and both the maleimides, it could still provide an estimation. Since this method quantifies maleimides directly, it might even be more accurate than Ellman's assay, which has to be reversed due to its focus on thiol detection.

5.3 Future Directions

Both of the functionalization methods developed in this thesis could be further improved via more thorough optimization. Firstly, different amounts of EDC and NHS could be compared to discover the molar ratio resulting in the best performance. Secondly, NHS and EDC might activate CNC-COO^- more effectively in its protonated form (CNC-COOH). This opportunity could be explored by treating CNC-COO^- with acid before dialysis. Thirdly, optimization of the conversion of CNC-SH to CNC-MAL in ethanol remained beyond the scope of this thesis, even though ethanol performed as a superior solvent compared to water.

With these improvements, the introduced CNC end-functionalizations could become effective and simple routes to produce CNCs that can regioselectively be reacted with thiol-reactive or thiol-containing molecule of choice. Particularly NHS/EDC-catalyzed thiolation displays high potential at introducing end-thiols with satisfactory yield. Even the conversion of CNC-SH to CNC-MAL can provide a potentially feasible source for thiol-reactive CNCs, after improving its yield. Potential thiol-containing molecules to couple with CNC-MAL include proteins with available cysteine residues. For example, hydrophobins with free cysteine could be attached to CNC ends to regioselectively modify CNCs into a form that behaves like a colloidal surfactant, as presented in Figure 12. Thus, CNCs would be modified into amphiphilic form in a gentler way compared to surface modifications that can damage the underlying crystalline structure.

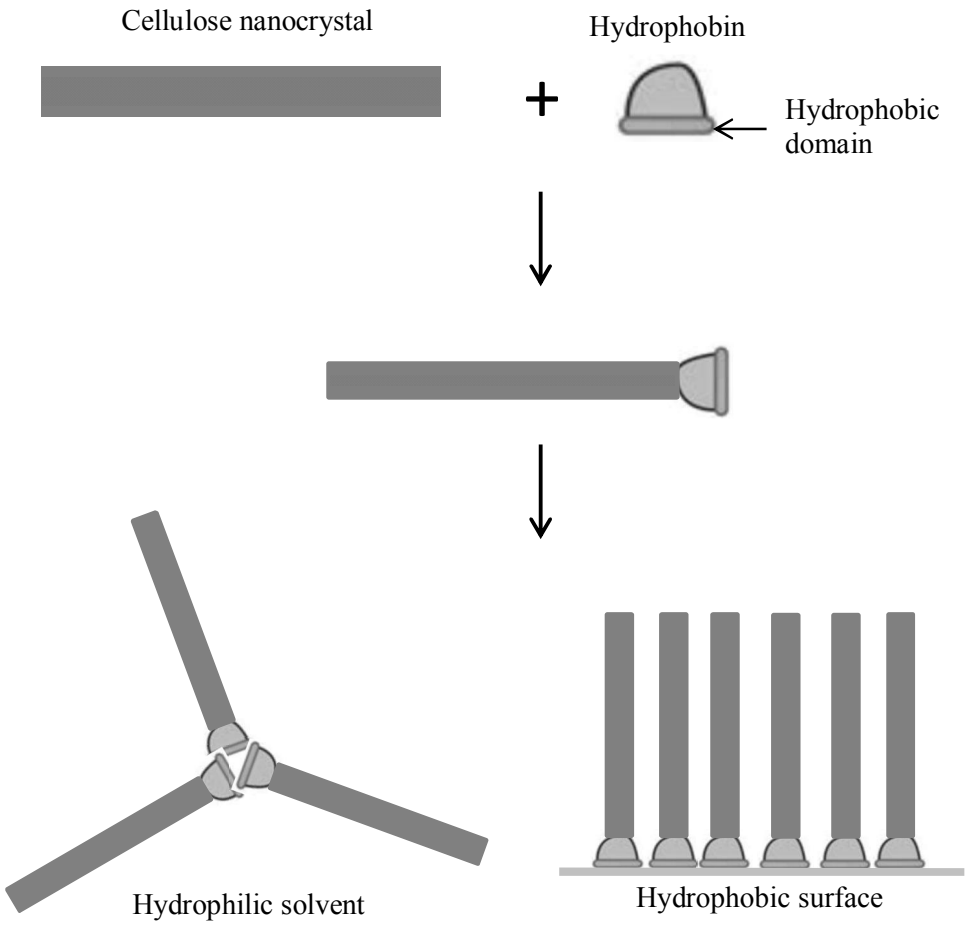

Figure 12: Possible effect of coupling a CNC with a hydrophobin.

6. Conclusions

This thesis executed the intended CNC functionalizations introduced in Chapter 1. According to adsorption studies with QCM-D, the end-thiolation of CNCs via NHS/EDC-catalyzed coupling between CNC-COO^- and NH_2-R-SH was successful. Among the alternative protocols compared, this reaction was found to proceed optimally when using EDC and NHS in a molar ratio of 10:1 and increasing the ionic strength of the NHS/EDC-activated CNC-COO^- suspension before introducing NH_2-R-SH. Essentially, this method functions as effectively as previously developed CNC end-thiolation via reductive amination. Furthermore, NHS/EDC-catalyzed end-thiolation can be accomplished at room temperature and faster than reductive amination.

In addition, adsorption studies with QCM-D and colorimetric quantification with Ellman's assay suggest that maleimide groups were introduced in CNCs via reacting CNC-SH with BM-PEG. According to the results, the optimal protocol for this reaction involves BM-PEG in a 50-fold molar excess compared to the estimated thiol concentration of CNC-SH. Performing the reaction in ethanol was found to stabilize thiol groups to preserve them available for BM-PEG. However, even in the optimized conditions, the yield of this functionalization was very small.

To conclude, CNCs can be end-functionalized on small scale in alternative ways to regioselectively modify their chemical behavior. Feasibility of these functionalizations remains to be explored along with the practical applications to use the resulting CNCs for. Essentially, end-functionalized CNCs represent artificially developed anisotropic colloids. Since the production of anisotropic colloids poses a prerequisite for engineered self-assembly, CNC end-functionalization can enable applications that both mimic the natural self-assembly mechanisms and are produced from a renewable and biocompatible raw material.

References

Ahn, B, Rhee, SG & Stadtman, ER 1987, 'Use of fluorescein hydrazide and fluorescein thiosemicarbazide reagents for the fluorometric determination of protein carbonyl groups and for the detection of oxidized protein on polyacrylamide gels', *Analytical Biochemistry*, vol 161, no. 2, p. 245–257.

Araki, J, Kuga, S & Magoshi, J 2002, ' Influence of reagent addition on carbodiimide-mediated amidation for poly(ethylene glycol) grafting', *Journal of Applied Polymer Science*, vol 85, no. 6, p. 1349-1352.

Ariura, F, Schappacher, M, Borsali, R & Deffieux, A 2009, 'Janus combs with polystyrene and poly(methyl vinyl ether) branches: Design, characterization and properties', *Reactive and Functional Polymers*, vol 69, no. 7, p. 402–408.

Arndt, P, Bockholt, K, Gerdes, R, Huschens, S, Pyplo, J, Redlich, H & Samm, K 2003, 'Cellulose oligomers: preparation from cellulose triacetate, chemical', *Cellulose*, vol 10, p. 75–83.

Azzam, F, Heux, L, Putaux, J-L & Jean, B 2010, 'Preparation By Grafting Onto, Characterization, and Properties of Thermally Responsive Polymer-Decorated Cellulose Nanocrystals', *Biomacromolecules*, vol 11, no. 12, p. 3652-3659.

Bentzen, EL, Tomlinson, ID, Mason, J, Gresch, P, Warnement, MR, Wright, D, Sanders-Bush, E, Blakely, R & Rosenthal, SJ 2005, 'Surface Modification To Reduce Nonspecific Binding of Quantum Dots in Live Cell Assays', *Bioconjugate Chemistry*, vol 16, no. 6, p. 1488-1494.

Cai, W, Zhang, X, Wu, Y & Chen, X 2006, 'A Thiol-Reactive ^{18}F-Labeling Agent, *N*-[2-(4-^{18}F-Fluorobenzamido)Ethyl]Maleimide, and Synthesis of RGD Peptide-Based Tracer for PET Imaging of $\alpha_v\beta_3$ Integrin Expression', *The Journal of Nuclear Medicine*, vol 47, no. 7, p. 1172-1180.

Chen, L, Chen, T, Fang, W, Wen, Y, Lin, S, Lin, J & Cai, C 2013, 'Synthesis and pH-Responsive “Schizophrenic” Aggregation of a Linear-Dendron-Like Polyampholyte Based on Oppositely Charged Polypeptides', *Biomacromolecules*, vol 14, no. 12, p. 4320–4330.

Dendukuri, D, Hatton, TA & Doyle, PS 2007, 'Synthesis and Self-Assembly of Amphiphilic Polymeric Microparticles', *Langmuir*, vol 23, no. 8, p. 4669–4674.

Enomoto-Rogers, Y, Kamitakahara, H, Yoshinaga, A & Takano, T 2011a, 'Water-soluble low-molecular-weight cellulose chains radially oriented on gold nanoparticles', *Cellulose*, vol 18, p. 929–936.

Enomoto-Rogers, Y, Kamitakahara, H, Yoshinaga, A & Takano, T 2011b, 'Synthesis of diblock copolymers with cellulose derivatives. 4. Self-assembled nanoparticles of amphiphilic cellulose derivatives carrying a single pyrene group at the reducing-end', *Cellulose*, vol 18, p. 1005–1014.

Enomoto-Rogers, Y, Kamitakahara, H, Yoshinaga, A & Takano, T 2012, 'Comb-shaped graft copolymers with cellulose side-chains prepared via click chemistry', *Carbohydrate Polymers*, vol 87, no. 3, p. 2237–2245.

Evans, DF & Wennerström, H 1999, *The colloidal domain: where physics, chemistry, biology, and technology meet*, 2nd edn, Wiley, New York.

Ge, Z, Xu, J, Hu, J, Zhang, Y & Liu, S 2009, 'Synthesis and supramolecular self-assembly of stimuli-responsive water-soluble Janus-type heteroarm star copolymers', *Soft Matter*, vol 5, no. 20, pp. 3932-3939.

Glasser, W & Becker, U 1999, 'About the depolymerization of cellulose propionate to segments with low DP', *Cellulose*, vol 6, p. 283–289.

Goffina, A-L, Raquez, J-M, Duquesnea, E, Siqueira, G, Habibi, Y, Dufresne, A & Dubois, P 2011, 'Poly(ε-caprolactone) based nanocomposites reinforced by surface-grafted cellulose nanowhiskers via extrusion processing: Morphology, rheology and thermo-mechanical properties', *Polymer*, vol 52, pp. 1532-1538.

Habibi, Y, Goffin, A-L, Schiltz, N, Duquesne, E, Dubois, P & Dufresne, A 2008, 'Bionanocomposites based on poly(ε-caprolactone)-grafted cellulose nanocrystals by ring-opening polymerization', *Journal of Materials Chemistry*, vol 18, pp. 5002-5010.

Habibi, Y, Lucia, LA & Rojas, OJ 2010, 'Cellulose Nanocrystals: Chemistry, Self-Assembly, and Applications', *Chemical Reviews*, vol 110, no. 6, p. 3479–3500.

Hall, DJ, Van Den Berghe, HM & Dove, AP 2011, 'Synthesis and post-polymerization modification of maleimide-containing polymers by 'thiol-ene' click and Diels–Alder chemistries', *Polymer International*, vol 60, no. 8, p. 1149–1157.

Hebeish, A & Guthrie, JT 1981, *The Chemistry and Technology of Cellulosic Copolymers*, Springer Berlin Heidelberg.

Hermanson, GT 1996, *Bioconjugate Techniques*, Academic Press, San Diego, California, USA.

Hieta, K, Kuga, S & Usuda, M 1984, 'Electron Staining of Reducing Ends Evidences a Parallel-Chain Structure in Valonia Cellulose', *Biopolymers*, vol 23, p. 1807-1810.

Hong, L, Jiang, S & Granick, S 2006, 'Simple Method to Produce Janus Colloidal Particles in Large Quantity', *Langmuir*, vol 22, no. 23, p. 9495–9499.

Jiang, K, Schadler, LS, Siegel, RW, Zhang, X, Zhang, H & Terrones, M 2004, ' Protein immobilization on carbon nanotubes *via* a two-step process of diimide-activated amidation', *Journal of Materials Chemistry*, vol 14, p. 37-39.

Jiang, S & Granick, S 2008, 'Controlling the Geometry (Janus Balance) of Amphiphilic Colloidal Particles', *Langmuir*, vol 24, no. 6, p. 2438–2445.

Kalashnikova, I, Bizot, H, Cathala, B & Capron, I 2011, 'New Pickering Emulsions Stabilized by Bacterial Cellulose Nanocrystals', *Langmuir*, vol 27, no. 12, pp. 7471-7479.

Kamitakahara, H & Nakatsubo, F 2005, 'Synthesis of diblock copolymers with cellulose derivatives. 1. Model study with azidoalkyl carboxylic acid and cellobiosylamine derivative.', *Cellulose*, vol 12, p. 209–219.

Karaaslan, MA, Gao, G & Kadla, JF 2013, 'Nanocrystalline cellulose/β-casein conjugated nanoparticles prepared by click chemistry', *Cellulose*, vol 20, p. 2655–2665.

Kasuya, N, Kasaka, Y, Habu, N & Ohnishi, A 2002, 'Development of chiral stationary phases consisting of low-molecular-weight cellulose derivatives covalently bonded to silica gel', *Cellulose*, vol 9, p. 263-269.

Kelly, JA, Shopsowitz, KE, Ahn, JM, Hamad, WY & MacLachlan, MJ 2012, 'Chiral Nematic Stained Glass: Controlling the Optical Properties of Nanocrystalline Cellulose-Templated Materials', *Langmuir*, vol 28, no. 50, p. 17256–17262.

Kim, DK, Mikhaylova, M, Zhang, Y & Muhammed, M 2003, 'Protective Coating of Superparamagnetic Iron Oxide Nanoparticles', *Chemistry of Materials*, vol 15, p. 1617-1627.

Klemm, D, Kramer, F, Moritz, S, Lindström, T, Ankerfors, M, Gray, D & Dorris, A 2011, 'Nanocelluloses: A New Family of Nature-Based Materials', *Angewandte Chemie International Edition*, vol 50, no. 24, p. 5438–5466.

Kostiainen, MA, Szilvay, GR, Smith, DK, Linder, MB & Ikkala, O 2006, 'Multivalent Dendrons for High-Affinity Adhesion of Proteins to DNA', *Angewandte Chemie International Edition*, vol 45, no. 21, p. 3538-3542.

Koyama, M, Helbert, W, Imai, T, Sugiyama, J & Henrissat, B 1997, 'Parallel-up structure evidences the molecular directionality during biosynthesis of

bacterial cellulose', *Proceedings of the National Academy of Sciences of the United States of America*, vol 94, no. 17, p. 9091–9095.

Laaksonen, P, Walther, A, Malho, J-M, Kainlaurii, M, Ikkala, O & Linder, MB 2011, 'Genetic Engineering of Biomimetic Nanocomposites: Diblock Proteins, Graphene, and Nanofibrillated Cellulose', *Angewandte Chemie*, vol 123, no. 37, p. 8847-8850.

Lanson, D, Ariura, F, Schappacher, M, Borsali, R & Deffieux, A 2009, 'Comb Copolymers with Polystyrene and Polyisoprene Branches: Effect of Block Topology on Film Morphology', *Macromolecules*, vol 42, no. 12, p. 3942–3950.

Li, M, De, P, Li, H & Sumerlin, BS 2010a, 'Conjugation of RAFT-generated polymers to proteins by two consecutive thiol-ene reactions', *Polymer Chemistry*, vol 1, p. 854–859.

Li, Z, Ma, J, Cheng, C, Zhang, K & Wooley, KL 2010b, 'Synthesis of Hetero-Grafted Amphiphilic Diblock Molecular Brushes and Their Self-Assembly in Aqueous Medium', *Macromolecules*, vol 43, no. 3, p. 1182–1184.

Linder, MB 2009, 'Hydrophobins: Proteins that self assemble at interfaces', *Current Opinion in Colloid & Interface Science*, vol 14, no. 5, p. 356–363.

Liu, B, Wei, W, Qu, X & Yang, Z 2008, 'Janus Colloids Formed by Biphasic Grafting at a Pickering Emulsion Interface', *Angewandte Chemie*, vol 47, no. 21, p. 3973–3975.

Lokanathan, AR, Nykänen, A, Seitsonen, J, Johansson, L-S, Campbell, J, Rojas, OJ, Ikkala, O & Laine, J 2013, 'Cilia-Mimetic Hairy Surfaces Based on End-Immobilized Nanocellulose Colloidal Rods', *Biomacromolecules*, vol 14, no. 8, p. 2807–2813.

Lowe, AB 2010, 'Thiol-ene "click" reactions and recent applications in polymer and materials synthesis', *Polymer Chemistry*, vol 1, p. 17-36.

Mao, Z, Xu, H & Wang, D 2010, 'Molecular Mimetic Self-Assembly of Colloidal Particles', *Advanced Functional Materials*, vol 20, no. 7, p. 1053-1074.

Mazzaglia, A, Bondi, ML, Scala, A, Zito, F, Barbieri, G, Crea, F, Vianelli, G, Mineo, P, Fiore, T, Pellerito, C, Pellerito, L & Costa, MA 2013, 'Supramolecular Assemblies Based on Complexes of Nonionic Amphiphilic Cyclodextrins and a *meso*-Tetra(4-sulfonatophenyl)porphine Tributyltin(IV) Derivative: Potential Nanotherapeutics against Melanoma', *Biomacromolecules*, vol 14, no. 11, p. 3820–3829.

Moon, RJ, Martini, A, Nairn, J, Simonsen, J & Youngblood, J 2011, 'Cellulose nanomaterials review: structure, properties and nanocomposites', *Chemical Society Reviews*, vol 40, no. 7, pp. 3941-3994.

Nakagawa, A, Kamitakahara, H & Takano, T 2012, 'Synthesis and thermoreversible gelation of diblock methylcellulose analogues via Huisgen 1,3-dipolar cycloaddition', *Cellulose*, vol 19, p. 1315–1326.

Nakagawa, A, Steiniger, F, Richter, W, Koschella, A, Heinze, T & Kamitakahara, H 2012, 'Thermoresponsive Hydrogel of Diblock Methylcellulose: Formation of Ribbonlike Supramolecular Nanostructures by Self-Assembly', *Langmuir*, vol 28, no. 34, p. 12609-12618.

Nie, Z, Li, W, Seo, M & Xu, S 2006, 'Janus and Ternary Particles Generated by Microfluidic Synthesis: Design, Synthesis, and Self-Assembly', *Journal of American Chemical Society*, vol 128, no. 29, p. 9408–9412.

Olszewska, AM, Kontturi, E, Laine, J & Österberg, M 2013, 'All-cellulose multilayers: long nanofibrils assembled with short nanocrystals', *Cellulose*, vol 20, p. 1777-1789.

Orelma, H, Filpponen, I, Johansson, L-S, Österberg, M, Rojas, O & Laine, J 2012, 'Surface Functionalized Nanofibrillar Cellulose (NFC) Film as a Platform for Immunoassays and Diagnostics', *Biointerphases*, vol 7, p. 1-12.

Pieper, JS, Hafmans, T, Veerkamp, JH & van Kuppelvelt, TH 2000, ' Development of tailor-made collagen–glycosaminoglycan matrices: EDC/NHS crosslinking, and ultrastructural aspects', *Biomaterials*, vol 21, no. 6, p. 581-593.

Pounder, RJ, Stanford, MJ, Brooks, P, Richards, SP & Dove, AP 2008, 'Metal free thiol –maleimide 'Click' reaction as a mild functionalisation strategy for degradable polymers', *Chemical Communications*, vol 44, no. 41, p. 5158-5160.

Rein, DM, Khalfin, R & Cohen, Y 2012, 'Cellulose as a novel amphiphilic coating for oil-in-water and water-in-oil dispersions', *Journal of Colloid and Interface Science*, vol 386, no. 1, p. 456–463.

Shang, W, Huang, J, Luo, H, Chang, PR, Feng, J & Xie, G 2013, 'Hydrophobic modification of cellulose nanocrystal', *Cellulose*, vol 20, p. 179–190.

Shopsowitz, KE, Hamad, WY & MacLachlan, MJ 2012, 'Flexible and iridescent chiral nematic mesoporous organosilica films', *Journal of American Chemical Society*, vol 134, p. 786-870.

Sipahi-Saglam, E, Gelbrich, M & Gruber, E 2003, 'Topochemically modified cellulose', *Cellulose*, vol 10, p. 237–250.

Sturcová, A, His, I, Apperley, DC, Sugiyama, J & Jarvis, MC 2004, 'Structural Details of Crystalline Cellulose from Higher Plants', *Biomacromolecules*, vol 5, no. 4, p. 1333–1339.

Taipina, MDO, Ferrarezi, MMF, Yoshida, IVP & Gonc¸alves, MDC 2013, 'Surface modification of cotton nanocrystals with a silane agent', *Cellulose*, vol 20, p. 217–226.

Varjonen, S, Laaksonen, P, Paananen, A, Valo, H, Hähl, H, Laaksonen, T & Linder, MB 2011, 'Self-assembly of cellulose nanofibrils by genetically engineered fusion proteins', *Soft Matter*, vol 7, p. 2402-2411.

Velleste, R, Teugjas, H & Väljamäe, P 2010, 'Reducing end-specific fluorescence labeled celluloses for cellulase mode of action', *Cellulose*, vol 17, p. 125–138.

Vercelli, B & Zotti, G 2007, 'Star-Shaped and Linear Terthiophene-thiol Self-assembled Monolayers as Scaffolds for Gold Nanoparticles', *Chemistry of Materials*, vol 19, no. 3, p. 443–452.

Walther, A & Müller, AHE 2013, 'Janus particles', *Chemical Reviews*, vol 113, p. 5194−5261.

Wei, K, Su, L, Chen, G & Jiang, M 2011, 'Does PNIPAM block really *retard* the micelle-to-vesicle transition of its copolymer?', *Polymer*, vol 52, no. 16, p. 3647–3654.

Yamane, C, Aoyagi, T, Ago, M, Sato, K, Okajima, K & Takahashi, T 2006, 'Two Different Surface Properties of Regenerated Cellulose due to Structural Anisotropy', *Polymer Journal*, vol 38, no. 8, p. 819-826.

Yoshitake, S, Yamada, Y, Ishikawa, E & Masseyeff, R 1979, 'Conjugation of Glucose Oxidase from *Aspergillus niger* and Rabbit Antibodies Using *N*-Hydroxysuccinimide Ester of *N*-(4-Carboxycyclohexylmethyl)-Maleimide', *European Journal of Biochemistry*, vol 101, no. 2, p. 395-399.

Yu, H-Y & Qin, Z-Y 2014, 'Surface grafting of cellulose nanocrystals with poly(3-hydroxybutyrate-co-3-hydroxyvalerate)', *Carbohydrate Polymers*, vol 101, p. 471–478.

Zhang, J, Jin, J & Zhao, H 2009, 'Surface-Initiated Free Radical Polymerization at the Liquid−Liquid Interface: A One-Step Approach for the Synthesis of Amphiphilic Janus Silica Particles', *Langmuir*, vol 25, no. 11, p. 6431–6437.

Zhao, Y, Sakai, F, Su, L, Liu, Y, Wei, K, Chen, G & Jiang, M 2013, 'Progressive Macromolecular Self-Assembly: From Biomimetic Chemistry to Bio-Inspired Materials', *Advanced Materials*, vol 25, p. 5215-5256.

Zoppe, JO, Habibi, Y, Rojas, OJ, Venditti, RA, Johansson, L-S, Efimenko, K, Österberg, M & Laine, J 2010, 'Poly(*N*-isopropylacrylamide) Brushes Grafted from Cellulose Nanocrystals via Surface-Initiated Single-Electron Transfer Living Radical Polymerization', *Biomacromolecules*, vol 11, no. 10, p. 2683–2691.

Zoppe, JO, Österberg, M, Venditti, RA, Laine, J & Rojas, OJ 2011, 'Surface Interaction Forces of Cellulose Nanocrystals Grafted with Thermoresponsive Polymer Brushes', *Biomacromolecules*, vol 12, no. 7, p. 2788-2796.

Zou, J, Guan, B, Liao, X, Jiang, M & Tao, F 2009, 'Dual Reversible Self-Assembly of PNIPAM-Based Amphiphiles Formed by Inclusion Complexation', *Macromolecules*, vol 42, no. 19, p. 7465–7473.

Cysteine Standard for Ellman's Assay

Cysteine solutions were prepared with concentrations of 100 µM, 50 µM, 30 µM and 10 µM in buffer (0.1 mM NaH_2PO_4, 1 mM EDTA, pH 8). Each solution was mixed with 50 µl of Ellman's reagent solution (4 mg of Ellman's reagent in 1 ml of similar buffer). After a 15-min incubation, the absorbance of each solution for UV light at a wavelength of 412 nm was measured. The device was reset using only the buffer as a baseline solution. From the results, the corresponding absorbance by a blank solution without cysteine was subtracted.

The measurements were repeated three times for each concentration to establish standard 1. In addition, standard 2 was prepared to mitigate the effects of cysteine degradation during the assay upon exposure to dissolved oxygen (Hermanson 1996). Standard 2 was prepared similarly to standard 1. As the sole difference, instead cysteine solution was not used fresh but after an incubation of 5 days. For each concentration of the incubated cysteine solution, absorbance measurements with Ellman's reagent were repeated once.

In order to determine the appropriate standard plot to base calculations on, a test point absorbance was measured right after each measurement of the absorbance by CNC-MAL + cys. The test point sample included 50 µM of cysteine and was prepared and measured similarly to the corresponding solution in standard 1. For compatibility with CNC-MAL + cys, 33% of the buffer was replaced with ethanol in the sample as well as its blank and baseline solutions.

The measured absorbance values for all the standards and test points are presented as a function of cysteine concentration in Figure 13. As seen in this figure, the absorbance increases with increasing cysteine concentration approximately linearly for both standards. However, standard 2 has all its absorbance values below those of standard 1. This implies that the UV absorbance at 412 nm by cysteine with Ellman's reagent significantly decreases when using partially degraded cysteine. Thus, standard 2 could function as an adjusted standard for samples including similarly degraded cysteine.

The standard plots have slopes of 0.0098 μM^{-1} for standard 1 (R^2 = 0.9491) and 0.0021 μM^{-1} for standard 2 (R^2 = 0.9973). The correct values to use as $\Delta A_{cys}/\Delta c_{cys}$ when estimating the maleimide concentration of CNC-MAL with equation (4) were selected by observing the locations of the test points in relation to the standard plots. Test point 1 (measured right after the first measurement of CNC-MAL + cys) falls close to standard 1, whereas test point 2 (measured right after the second measurement of CNC-MAL + cys) approaches standard 2. Thus, the slope of standard 1 was selected for calculations based on the first absorbance measurement of CNC-MAL + cys and the slope of standard 2 for calculations based on the second one.

The positions of the test points in relation to the standard plots are potentially influenced by the timing of the measurement repetitions. The absorbance value at test point 2 was acquired later than that of test point 1. Therefore, part of the cysteine had possibly already degraded by that time. However, the degradation would unlikely proceed as far during one repetition of measurements as during an incubation of five days that standard 2 completed. Nevertheless, standard 2 was used to approximate the ratio between absorbance and thiol concentration of CNC-MAL during its second absorbance measurement.

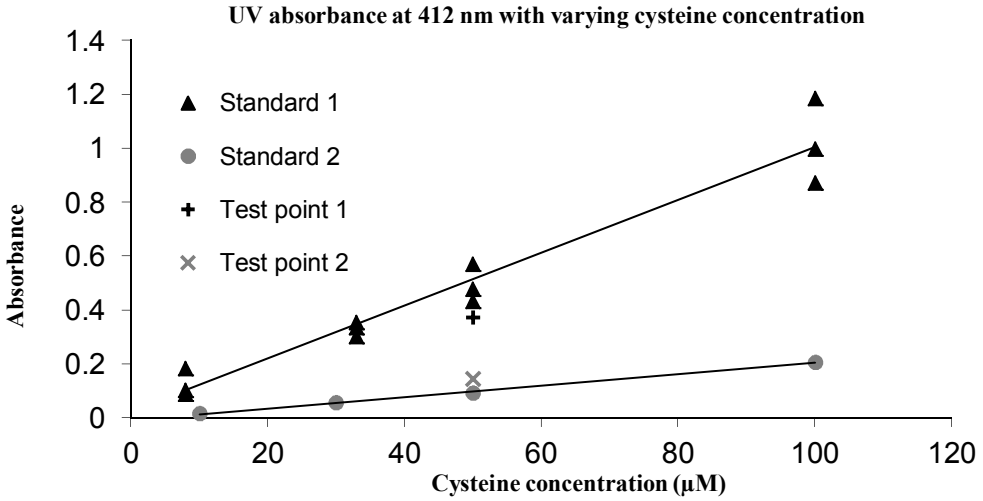

Figure 13: Cysteine standard plots and test points for Ellman's assay.